ASME Journal of Turbomachinery
Online journal at:
https://asmedigitalcollection.asme.org/turbomachinery

Fundamentals of Scaling of Overall Cooling Effectiveness With Temperature Ratio

James Cartlidge
Department of Engineering Science,
University of Oxford,
Parks Road,
Oxford OX1 3PJ, UK
e-mail: james.cartlidge@eng.ox.ac.uk

Thomas Povey[1]
Department of Engineering Science,
University of Oxford,
Parks Road,
Oxford OX1 3PJ, UK
e-mail: thomas.povey@eng.ox.ac.uk

In this paper we study the relationship between overall cooling effectiveness (or so-called metal effectiveness) and mainstream-to-coolant total temperature ratio (TR), for typical high-pressure nozzle guide vane (HPNGV) cooling systems. The temperature ratio range studied is that between typical experimental conditions (TR ≅ 1.2) and typical engine conditions (TR ≅ 2.0). The purpose is twofold: firstly, to quantify the difference in overall cooling effectiveness between experimental and engine conditions of temperature ratio; and—secondly—to understand the physical bases for the difference, separated in terms of changes in five local surface boundary conditions. We do this using a bespoke conjugate thermal model which includes models of both the internal cooling and the external film cooling layer. Three typical cooling architectures are studied. The results allow comparison and scaling between situations at different conditions of temperature ratio.
[DOI: 10.1115/1.4063730]

Keyword: fluid dynamics and heat transfer phenomena in compressor and turbine components of gas turbine engines, heat transfer, film cooling

Introduction

In modern gas turbine engines, combustor outlet temperature can be as high as 2000 K. High-pressure nozzle guide vanes (HPNGVs) are typically cooled with a combination of internal cooling and film cooling. In HPNGV experiments, the measured surface temperatures are commonly expressed in non-dimensional form either as adiabatic film effectiveness, η_{aw} (typically when only film cooling is considered), or overall cooling effectiveness, θ (typically when both internal cooling and film cooling is considered). These parameters are commonly defined by

$$\eta_{aw}(x) = \frac{T_{01h} - T_{aw}(x)}{T_{01h} - T_{01c}} \tag{1}$$

and,

$$\theta(x) = \frac{c_h(x)T_{01h} - T_{w1}(x)}{c_h(x)T_{01h} - c_c(x)T_{02c}} \tag{2}$$

where T_{01h} is mainstream total temperature, $T_{aw}(x)$ is adiabatic wall temperature, T_{01c} is coolant temperature at the cooling hole outlet, $c_h(x)$ is mainstream recovery ratio, $T_{w1}(x)$ is wall external surface temperature, $c_c(x)$ is the local recovery ratio of a *hypothetical unmixed coolant stream with adiabatic wall condition* and total pressure and temperature equal to those of the coolant at plane 1, and T_{02c} is total temperature at the cooling system inlet.

Sets of non-dimensional groups for *adiabatic film effectiveness*, $\eta_{aw}(x)$, have been developed by Ornano and Povey [1], Eckert [2], Baldauf and Scheurlen [3] and Greiner et al. [4]. Ornano and Povey [1] emphasise the inclusion of temperature ratio ($TR = T_{01h}/T_{02c}$) as a non-dimensional group because of its significance in determining adiabatic film effectiveness. We return to this point later.

There have been fewer studies of the scaling of the overall cooling effectiveness problem. Luque et al. [5] define the fully cooled gas turbine flow field in terms of the following 19 variables: p_{01h}, ρ_{1h}, μ_{1h}, k_{1h}, c_{p1h}, γ_{1h}, p_{02c}, ρ_{2c}, μ_{2c}, k_{2c}, c_{p2c}, γ_{2c}, p_3, y, C_x, k_w, T_{01h}, T_{02c}, T_{w1}. Here p_{01h}, ρ_{1h}, μ_{1h}, k_{1h} and γ_{1h} are total pressure, density, dynamic viscosity, thermal conductivity, specific heat capacity at constant pressure and ratio of specific heat capacities (c_p/c_v) of the mainstream at inlet conditions. Likewise, p_{02c}, ρ_{2c}, μ_{2c}, k_{2c} and γ_{2c} are the corresponding variables for coolant at the cooling channel inlet condition. The remaining variables are: the domain-exit static pressure, p_3; the surface-normal distance, y; the characteristic length (the plate surface length of the HPNGV in the current study), C_x; and the wall thermal conductivity, k_w. Luque et al. [5] show that these can be reduced to 18 variables of which two are temperature differences: p_{01h}, ρ_{1h}, μ_{1h}, k_{1h}, c_{p1h} γ_{1h}, p_{02c}, ρ_{2c}, μ_{2c}, k_{2c}, c_{p2c}, γ_{2c}, p_3, y, C_x, k_w, $T_{02c} - T_{\Re}$, $T_{w1} - T_{\Re}$, were $T_{\Re}$ is the recovery and redistribution temperature (we explore this further in a moment). These are subsequently reduced via a process of dimensional analysis to 13 non-dimensional quantities

$$\theta,\ \frac{C_x\sqrt{p_{01h}\rho_{1h}}}{\mu_{1h}},\ \frac{c_{p1h}\mu_{1h}}{k_{1h}},\ \frac{p_{02c}}{p_{01h}},\ \frac{p_{01h}}{p_3},$$
$$\frac{\rho_{2c}}{\rho_{1h}},\ \frac{\mu_{2c}}{\mu_{1h}},\ \frac{k_{2c}}{k_{1h}},\ \frac{c_{p2c}}{c_{p1h}},\ \frac{y}{C_x},\ \frac{k_w}{k_{1h}},\ \gamma_{1h},\ \gamma_{2c}$$

The first five non-dimensional groups are, in turn: the overall cooling effectiveness, θ; the mainstream Reynolds number, Re_{1h};

[1]Corresponding author.
Manuscript received January 17, 2023; final manuscript received August 11, 2023; published online October 31, 2023. Assoc. Editor: James L. Rutledge.

the mainstream Prandtl number, Pr_{1h}; the coolant-to-mainstream pressure ratio, CMPR; and the domain pressure ratio, PR. The remaining seven groups have self-evident meanings based on the variables they contain.

For HPNGV laboratory experiments, a typical value of mainstream-to-coolant temperature ratio is TR = 1.2 (see, for example, Kirollos et al. [6]). This is lower than the typical engine value of TR = 2.0. A general problem arises when TR is varied, in that the non-dimensional groups of the system change in a complex inter-related way. It is common in experiments to attempt to match Re_{1h}, Pr_{1h}, CMPR and PR to engine conditions (see, for example, Kirollos et al. [6]). Geometric similarity constraints might also mean that y/C_x is matched. Although these five important non-dimensional groups might be matched, if TR is not matched to the engine condition, it is likely that the remaining seven non-dimensional groups will be unmatched. As overall cooling effectiveness is a function of all 12 remaining groups, it would be unnatural to expect it to take the same value as at the fully matched condition. If all 12 groups cannot be matched in practice between two situations of different TR, it is necessary to know how θ scales with the remaining 7 groups. Expressed in this way the problem is prima facie complex. The purpose of this paper is to explore a practical way forward with this scaling problem.

One of the first studies to seriously explore the issue of scaling overall cooling effectiveness with TR is that of Luque et al. [5]. The key question addressed in this paper was the impact of compressibility, and in particular the issue of compressibility effects even with the apparently incompressible cooling system ducts on account of coupling with compressible (external) regions of the flow. This problem had not previously been addressed, and the authors proposed a new TR-invariant definition of overall cooling effectiveness, θ'' (see Results VIII), based on a *recovery and redistribution temperature*. Using a conjugate low-order thermal model, they demonstrated exact collapse of θ'' for the special case of varying TR *with all other non-dimensional groups fixed to reference values.* The authors also showed experimentally [7] that for temperature ratios in the range $1.05 \leq TR \leq 1.22$ a good collapse of experimental data could be achieved in practice. The result of [7] was likely only possible because the TR range was limited, and thus changes in other non-dimensional groups were small. Taken together, these papers demonstrate the conceptual importance of the recovery and redistribution temperature, but it is difficult to know how to use this result in practice over wide TR ranges in systems in which non-dimensional groups are allowed to *vary sympathetically* with TR. It is these real systems that are the subject of this paper, and the key distinction with previous work.

We introduce three approaches that could be used to study the impact of TR on overall cooling effectiveness or adiabatic film effectiveness. We see examples of the first two in literature and argue that the third is new. They are:

(1) *Approach 1: perturb multiple non-dimensional groups simultaneously*. Identify all system variables and derive the set of non-dimensional groups that fully define θ or η_{aw}. Perturb several groups simultaneously and quantify and explain changes in θ or η_{aw} in terms of the combined effect of changes in each non-dimensional group. This process has been used extensively in the literature (often because the interrelationship between the non-dimensional groups is not understood) to attempt to understand the effect of particular non-dimensional groups on both θ and η_{aw} (see, for example, [4] and [8–13]). We dislike this approach because it is very difficult to understand the individual contribution of each non-dimensional group and therefore the physical interpretation is unclear. The impact of one group on θ and η_{aw} is often contaminated with the effect of an uncontrolled change in another non-dimensional group.

(2) *Approach 2: perturb each non-dimensional group individually*. Identify all system variables and derive the set of non-dimensional groups that fully define θ or η_{aw}. *Here, we must include TR as a non-dimensional group*. Perturb each non-dimensional group individually, whilst remaining groups take unchanged values. Quantify and explain the change in effectiveness in terms of variations in each non-dimensional group, in isolation of all other non-dimensional groups. This is the approach used by Ornano and Povey [1] for the study of the impact of TR on η_{aw}. We regard this as an important approach to best separate fundamental effects, but has two failings in practice for the problem of the impact of TR on θ: firstly it is unclear whether it is possible to find a choice of underlying variables that allow this process in practice; secondly, the set of non-dimensional groups is so large, it is arguable that non-sympathetic variation of all groups with TR renders the results so abstract as to be meaningless in practice.

(3) *Approach 3: virtual experiment with all variables and non-dimensional groups following TR sympathetically.* Describe system in terms of system variables, domain-global boundary conditions (BCs) and cooling system BCs (discussion later). Perform virtual experiments at a range of TRs with solutions fully converged, such that all system variables and non-dimensional groups vary sympathetically with TR. Output θ trends at different TRs. Explain results in terms of changes in underlying variables, underlying non-dimensional groups, or in terms of local surface boundary conditions (full discussion later). This is the approach we adopt in this paper. We argue that it is the only approach that is both tractable and provides results that are non-conflated with undesired changes in uncontrolled variables.

Studies that have used approach 1 include the following. Sweeney and Rhodes [8] studied impact of CMPR on θ with fixed TR and PR. Albert and Bogard [9] studied the impact of blowing ratio with fixed density ratio on $\bar{\eta}_{aw}$ and $\bar{\theta}$. Greiner et al. [4] numerically studied the impact of simultaneously varying multiple non-dimensional groups on η_{aw}. Rutledge et al. [10] showed numerically that, when blowing ratio ($u_{1c}\rho_{1c}/u_{1h}\rho_{1h}$), density ratio ($\rho_{1c}/\rho_{1h}$), momentum flux ratio ($\rho_{1c}u_{1c}^2/\rho_{1h}u_{1h}^2$) and velocity ratio ($u_{1c}/u_{1h}$) are fixed, η_{aw} is insensitive to variations in the remaining non-dimensional groups. Fischer et al. [11] and McNamara et al. [12] demonstrated experimentally that, when heat capacity flux ratio ($\rho_{1c}u_{1c}c_{p1c}/\rho_{1h}u_{1h}c_{p1h}$) is fixed and momentum flux ratio is constrained to the range $\rho_{1c}u_{1c}^2/\rho_{1h}u_{1h}^2 \leq 0.6$, η_{aw} is insensitive to variations in the remaining non-dimensional groups. Bryant and Rutledge [13] numerically studied the impact of η_{aw} on θ for matched h_m/h_c and Biot number. We have expressed our reservations about all studies that fall under approach 1.

The only study we know of that has used approach 2 is that of Ornano and Povey [1]. The authors numerically studied the sensitivity of η_{aw} to momentum flux ratio, specific heat capacity flux ratio, blowing ratio and TR. Specific BCs were chosen that allowed each non-dimensional group to be *individually* perturbed. The study was unique in this respect. This was important because individual results were not conflicted with undesired changes in other non-dimensional groups. The effect of each non-dimensional group was quantified in three distinct regions of increasing distance from the film cooling hole, which they referred to as binary, intermediate and mixed-out regions. The individual effect of each group on η_{aw} was explained with reference to the underlying physics. They showed that in the binary region the primary influence on η_{aw} was the momentum flux ratio, because it determines the initial trajectory of the cooling film. In the vicinity of the film cooling row, the mainstream and coolant flows are unmixed and therefore it is the flow *structure* that is of primary importance. Heat capacity flux ratio dominated changes in η_{aw} in the intermediate and mixed-out regions as this parameter determines the relative ability of the coolant and entrained hot-gas flow to store heat. Blowing ratio significantly affected η_{aw} in the intermediate region

as it governs the *initial* velocity ratio (u_{1c}/u_{1h}) or volume flow rate ratio and therefore determines the rate of shear interaction between coolant and mainstream, which influences the heat capacity flux ratio *within* the mixing layer. The effect of TR, *when all other non-dimensional groups were fixed*, was second order and attributed to induced changes in the density of the mixing layer, which has the affect of changing the kinematic viscosity (which governs the extent of near-wall mixing) and the volume dilation (which determines the extent to which turbulent flow structures are pushed into the mainstream). We believe that this work is important because it was the first study to truly isolate the *independent* effect of the key non-dimensional groups on η_{aw}. In many previous studies (approach 1 studies) the co-dependence of the non-dimensional groups was not fully appreciated, rendering the results difficult to interpret.

In our study, we wish to quantify and explain the change in overall cooling effectiveness with TR. We use a low-order conjugate thermal model which includes physics-based models of both the internal cooling and the external film cooling layer, and realistic gas and wall thermal properties. Predictions are performed for converged conjugate thermal systems at a range of temperature ratios, with boundary conditions set such that *all non-dimensional groups vary simultaneously and sympathetically with TR as they would in a real environment* subject to the same boundary conditions. The resulting trends of θ with TR represent the natural change of the entire thermal system with TR, subject to particular boundary conditions. We decompose contributions to the change in θ with TR into effects arising from five *local-surface boundary conditions* (discussion later): effectiveness of the mixing layer, η_{ML}; local through-wall-average wall thermal conductivity, $\bar{k}_w$; external heat transfer coefficient, h_m; internal heat transfer coefficient, h_c; and internal cooling effectiveness, λ. These five parameters form a complete set that describe θ for a zero-dimensional system. We refer to this as approach 3.

Under approach 3, instead of attempting to decompose the change in θ with TR in terms of these five local surface boundary conditions, we could have attempted to do so in terms of either the underlying dimensional variables, or the resulting non-dimensional groups. This would be practically challenging because of the number of variables in each case, and would give rise to complex and un-intuitive results non open to meaningful interpretation.

We now reiterate the rational for our approach, which is perhaps the most important point of this paper. In many studies that purport to study the effect of non-dimensional groups on θ or η_{aw}, we feel there is confusion and ambiguity about which non-dimensional groups had controlled (deliberate) or un-controlled (often unintended) variation. The problem is intrinsic in many experimental studies in that it is impossible in practice to vary one non-dimensional group whilst keeping all others constant. On close reading of the literature, it appears that in most experimental and numerical studies this problem was simply overlooked. We refer to studies with uncontrolled variation of certain non-dimensional groups as approach 1, and feel studies in this category are difficult to meaningfully interpret. Approach 2, in which individual non-dimensional groups are *individually varied*, may be desired from a very fundamental perspective, but we find this problem intractable, and of limited practical use both because of the very large number of non-dimensional groups, and because *independent variation* of non-dimensional groups is non-representative of real systems. In approach 3, all non-dimensional groups vary naturally and sympathetically with TR as they would in a real system. Approach 3 requires very careful attention to boundary conditions, a subject which we address in detail in the next section. The result of an approach 3 study would be a characteristic of θ or η_{aw} with TR. The contributions to this characteristic can be decomposed in three primary ways, and we advocate doing so in terms of so-called local-surface boundary conditions because we feel this is the only approach that allows clear physical interpretation.

Three Levels of Boundary Conditions

Before describing details of the numerical model we define three levels of boundary condition in our study, which we refer to as *domain-global* BCs, *cooling system* BCs, and *local surface* BCs. These are illustrated in Fig. 1. We emphasise that the results of our study have meaning only in the context of a precisely-defined set of boundary conditions—another key point of this paper.

Firstly, by the term *domain-global BCs* we refer to the boundary conditions on the mainstream flow for the implied NGV row, i.e. the conditions established in a particular experimental test facility or engine test. We perform studies for two types of domain-global BC, which represent the common ways of running experiments, namely:

(i) Fixed domain inlet-to-exit total-to-static pressure ratio, PR = 1.75, with fixed atmospheric exit pressure, $p_3 = 1.0$ bar. This is typical of facilities without independent backpressure control, and implies a fixed inlet total pressure ($p_{01h} =$ 1.75 bar). With varying TR, this implies variation in exit—and therefore surface—Reynolds number Re_{3h} by a factor of approximately 2.0 across the TR range tested (for TR = 2.0, $Re_{3h} = 0.97 \times 10^6$; for TR = 1.2, $Re_{3h} = 1.9 \times 10^6$).
(ii) Fixed exit Reynolds number (typical of facilities with independent back-pressure control) *and* fixed PR. This implies inlet pressure variation in the range 0.88 − 1.75 bar (fixed Re_{3h}) for TR in the range $1.2 \leq TR \leq 2.0$.

We note that, to compare trends of results subject to the two methods for setting domain-global boundary condition, we need to choose a condition at which to match Re_{3h}. We do this, somewhat arbitrarily, at the reference temperature conditions, TR = 2.0.

Second, by *cooling system BCs*, we refer to the boundary conditions for the cooling system, that in conjunction with the domain-global BCs, set the coolant-to-mainstream pressure ratio (CMPR) and TR. Here we refer to the coolant inlet total pressure (p_{02c}) and total temperature (T_{02c}) and the corresponding values for the mainstream (p_{01h} and T_{01h}) that satisfy a particular domain-global BC approach. A schematic of the domain is shown in Fig. 2 with the boundary conditions marked. We note three planes of interest: plane 1, the inlet plane and point of coolant injection into the mainstream; plane 2, the inlet to the reverse-pass coolant duct; plane 3, the outlet plane.

In all simulations we set the coolant inlet total temperature to $T_{02c} = 300$ K. To achieve TR in the range $1.2 \leq TR \leq 2.0$, the mainstream total temperature is varied in the range 360−600 K. CMPR (based on inlet values) has a fixed value of 1.025 for all simulations. To first order, this means that coolant-to-mainstream momentum flux ratio ($\rho_{1c}u_{1c}^2/\rho_{1h}u_{1h}^2$) is the same between simulations at different TR. Second order differences arise, however, due to, for example: changes in duct pressure loss that reduce the coolant total pressure at the coolant hole inlet; changes due to real-gas-effects in the mainstream and coolant ratios of specific heat capacities (γ_h and γ_c) that affect (very slightly) the local external Mach number distribution even for fixed domain-global PR. Nearly-constant coolant-to-mainstream momentum flux ratio across a wide range of TR implies a fairly wide range of heat

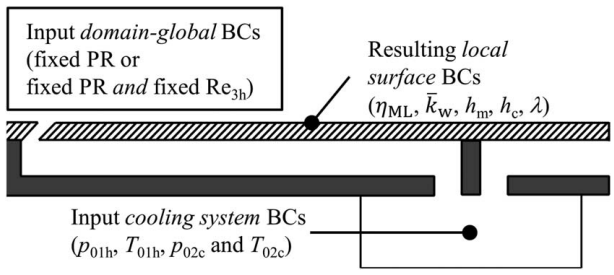

Fig. 1 Schematic of the three levels of boundary conditions

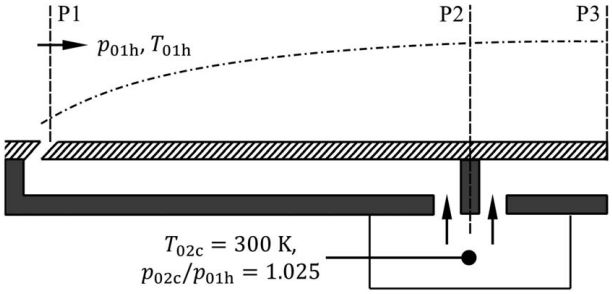

Fig. 2 Schematic of cooling system BCs and locations of planes 1–3

capacity flow rate ratio, $\dot{m}_{1c}c_{p1c}/\dot{m}_{1h}c_{p01h}$: essentially, if $\rho_{1c}u_{1c}^2/\rho_{1h}u_{1h}^2$ is approximately constant with TR, but ρ_{1c}/ρ_{1h} varies widely with TR, then the term $\rho_{1c}u_{1c}/\rho_{1h}u_{1h}$—which appears in the heat capacity flow rate ratio—must also vary widely. This change in heat capacity flow rate ratio is of primary importance in our system because it changes the effectiveness of the mixing layer. This effect is discussed in detail in [1]. Secondary effects arise due to changes in, for example: internal heat transfer coefficient driven by changes in channel velocity and local fluid properties.

Domain-global and cooling system boundary conditions at the reference TR, the resulting mass flow rate ratios, and geometric details of the system are summarized in Table 1. Conditions for all three cooling system networks are identical at the reference TR, with the exception of the coolant-to-mainstream mass flow rate ratios for the leading circuit, which take values within 3.8% of each other. These small differences arise because of small differences in cooling mass flow caused by differences in pressure drop between the cooling system inlet and exit.

Finally, by the local surface BCs we refer to the local boundary conditions that *result* on the surface in a converged simulation. Here we specifically refer to the surface distributions of five parameters: effectiveness of the mixing layer, η_{ML}; local through-wall-average wall thermal conductivity, $\bar{k}_w$; external heat transfer coefficient, h_m; internal heat transfer coefficient, h_c; and internal cooling effectiveness, λ. We justify this choice of boundary conditions in the next section.

Five Local Surface Boundary Conditions

In this section, we define the five *local-surface BCs* we reference in our study and provide justification for their choice.

Effectiveness of the Mixing Layer. Effectiveness of the mixing layer is the non-dimensional mixing layer recovery temperature or, equivalently, the non-dimensional driving temperature for heat transfer. We define this by

$$\eta_{ML}(x) = \frac{c_h(x)T_{01h} - c_m(x)T_{0m}(x)}{c_h(x)T_{01h} - c_c(x)T_{02c}} \tag{3}$$

where $T_{0m}(x)$ is the mixing layer total temperature and $c_m(x)$ is the mixing layer local recovery ratio. Recovery ratios are calculated using the stream conditions of total pressure and temperature, gas properties, and a local static pressure calculated by treating the boundary of the mixing layer (or, for $c_c(x)$, the boundary of the unmixed coolant stream) as a *slip line*, zero static pressure gradient in the wall-normal (or, approximately, slip-line-normal) direction. This process is discussed in more detail in the context of the numerical solver. We take an isentropic flow assumption for Mach number, and assume the turbulent flow correlation for recovery factor, $r(x) = \mathrm{Pr}^{1/3}(x)$. By defining Eq. (3) in this way—with individual local recovery ratios for each term—we constrain η_{ML} between 0 and 1. This is so because of the following theoretically limiting temperatures: a theoretical maximum external temperature of $c_h(x)T_{01h}$ in the case of no cooling flow and an adiabatic wall; a theoretical minimum external temperature of $c_c(x)T_{02c}$ for the case of perfect cooling (no entrained hot gas) and an adiabatic wall.

Local Through-Wall-Average Wall Thermal Conductivity. Wall thermal conductivity, $k_w(x, y)$, is evaluated at the local wall temperature, $T_w(x, y)$. We define the local through-wall-average wall thermal conductivity by

$$\bar{k}_w(x, y) = \frac{1}{t_w}\int_0^{t_w} k_w(x, y)\mathrm{d}y \tag{4}$$

where t_w is wall thickness.

External Heat Transfer Coefficient. The local external heat transfer coefficient is based on local fluid properties and length scale, and is defined by

$$h_m(x) = \frac{\mathrm{Nu}_m(x)k_m(x)}{x} \tag{5}$$

where $\mathrm{Nu}_m(x)$ is the local external Nusselt number distribution and $k_m(x)$ and is the local thermal conductivity of the gas in the mixing layer. We present a correlation for this later.

Table 1 Domain-global and cooling system boundary conditions at the reference TR, resulting mass flow rate ratios, and geometric details of the system

Boundary/operating conditions at reference TR		Value
Coolant plenum total temperature, T_{02c} (K)		300
Mainstream total temperature, T_{01h} (K)		600
Mainstream-to-coolant TR, (−)		2.0
Mainstream inlet Mach number, M_{1h} (−)		0.30
Mainstream exit Mach number, M_{3h} (−)		0.93
Coolant plenum total pressure, p_{02c} (bar)		1.79
Mainstream inlet total pressure, p_{01h} (bar)		1.75
Exit static pressure, p_3 (bar)		1.0
CMPR, p_{02c}/p_{01h} (−)		1.025
Coolant-to-mainstream mass flow rate ratio for reverse-pass cooling duct $\dot{m}_{1c}/\dot{m}_{1h}$ (−)	System 1	0.079
	System 2	0.082
	System 3	0.079
Coolant-to-mainstream mass flow rate ratio for the TE slot, $\dot{m}_{3c}/\dot{m}_{1h}$ (−)		0.019
Plate surface length, C_x (mm)		100
Plate width, w (m)		1
Wall thickness, t_w (mm)		1
Mainstream exit Re number, Re_{3h} (−)		0.97×10^6

Internal Heat Transfer Coefficient. In like manner, the local internal (cooling-channel) heat transfer coefficient is defined by

$$h_c(x) = \frac{\mathrm{Nu}_c(x) k_c(x)}{D(x)} \tag{6}$$

where $\mathrm{Nu}_c(x)$ is the local cooling channel Nusselt number and $k_c(x)$ the local thermal conductivity of the gas in the coolant channel. $D(x)$ is hydraulic diameter of the internal cooling channel. We present a correlation for this later.

Internal Cooling Effectiveness. The internal cooling effectiveness is the non-dimensional internal coolant temperature defined by

$$\lambda(x) = \frac{c_h(x) T_{01h} - T_{0c}(x)}{c_h(x) T_{01h} - c_c(x) T_{02c}} \tag{7}$$

where $T_{0c}(x)$ is the local internal coolant temperature, and where all other variables have been defined. In the absence of lateral conduction, defining $\lambda(x)$ in this way constrains $\lambda(x)$ between 0 and 1. This is so because of the following theoretically limiting temperatures: a theoretical maximum *local* internal coolant temperature equal to the local mainstream recovery temperature (i.e. $T_{0c}(x) = c_h(x) T_{01h}$); a theoretical minimum local internal coolant temperature equal to the local recovery temperature of a *hypothetical unmixed coolant stream with adiabatic wall condition* and total pressure and temperature equal to those of the coolant at plane 2 (i.e. $T_{0c}(x) = c_c(x) T_{02c}$). Both situations would arise in a system with very low cooling flow and high through-wall condition.

Justification for Choice of Local Surface Boundary Conditions. For a network with 1D conduction heat transfer in the through-wall direction (no lateral conduction), external wall surface temperature, T_{w1}, is given by

$$T_{w1} = c_m T_{0m} - \left(1 + \frac{h_m}{h_c} + \frac{h_m t_w}{k_w}\right)^{-1} \times (c_m T_{0m} - T_{0c}) \tag{8}$$

This is derived by equating the following heat transfer rate terms: convection from mixing layer to external wall; conduction in the through-wall direction; and convection from internal wall to coolant. By substituting Eqs. (2), (3) and (7) into Eq. (8) we arrive at the following expression for overall cooling effectiveness for systems with 1D conduction

$$\theta = \eta_{ML} + \frac{\lambda - \eta_{ML}}{1 + \dfrac{h_m}{h_c} + \mathrm{Bi}} \tag{9}$$

where Biot number is the ratio of wall thermal resistance to the effective convective thermal resistance, which we define by

$$\mathrm{Bi}(x) = \frac{h_m(x) t_w}{\bar{k}_w(x)} \tag{10}$$

By rearrangement this is equivalent to

$$\theta = \eta_{ML} + \frac{\lambda - \eta_{ML}}{1 + h_m\left(\dfrac{1}{h_c} + \dfrac{t_w}{\bar{k}_w}\right)} \tag{11}$$

We see that, for an incompressible 1D system, overall cooling effectiveness has the functional relationship $\theta = f(\eta_{ML}, \bar{k}_w, h_m, h_c, \lambda)$. In many real systems, the lateral conduction terms can be shown to be small compared to the surface-normal conduction terms. On this basis it can be argued that a decomposition of changes in θ with TR due to changes in each local surface BC—in isolation of changes in other local surface BCs—is sufficiently true for real systems that it can be used to give meaningful physical insight into the underlying mechanisms driving the relationship between θ and TR. We show later, by a linear-superposition check-sum approach that this simplification appears valid with reasonable accuracy for our actual systems.

Cooling System Network Definitions

We model the HPNGV as a flat plate with two internal coolant feeds, and ejection from a single row of film cooling holes located at a notional leading-edge point ($x/C_x = 0$; plane 1; see Fig. 2) and from a trailing edge (TE) slot ($x/C_x = 0.75$; plane 2; see Fig. 2). The TE slot feed is forward-pass (flowing in the same direction as the external flow) in the range $0.75 \le x/C_x < 1.00$. In the leading region of the plate ($0 \le x/C_x < 0.75$) the internal cooling flow is of reverse-pass design (see Kirollos and Povey [14]). We model three different systems:

(i) System 1, *point-inlet* reverse-pass. This is shown in Fig. 3(*a*). In this system there is a single feed and incremental heat pick-up along the channel. This system maximises the axial temperature variation of the coolant flow, but minimises the axial variation in wall temperature (see Kirollos and Povey [14]). Such a system is interesting both because it approaches a theoretical optimum for a cooling network, but also because it has complex coupling between internal cooling flow and the external mixing layer.

(ii) System 2, *distributed-inlet reverse-pass.* This is shown in Fig. 3(*b*). This system is one in which there is both incremental heat pick up in the flow direction, but also mass flow addition. The system can be thought of as representing a more open internal cooling system; i.e. *unguided* reverse-pass flow in the direction of the sink (coolant outlet).

(iii) System 3, *fully-mixed reverse-pass*. This is shown in Fig. 3(*c*). This is a theoretical system, not possible in practice, in which the temperature in the entire cooling duct is constant, and set to the mid-point of the inlet and outlet temperature. Conservation equations taking into account inlet flow, outlet flow, and heat transfer are satisfied for the *duct as a single entity*. This represents extreme (beyond physical limit) mixing of the internal cooling flow.

The purpose of studying three systems is to test the sensitivity of our general result to the specific cooling system network. We

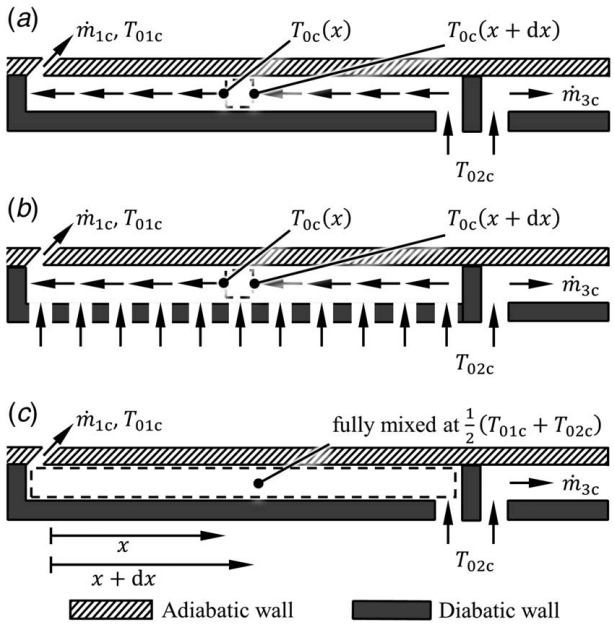

Fig. 3 Cooling systems considered in the current study: (*a*) system 1, point-inlet reverse-pass; (*b*) system 2, distributed-inlet reverse-pass; (*c*) system 3, fully-mixed reverse-pass

discuss the correlations for internal heat transfer coefficients and internal cooling pressure loss in the next sections.

Details of the Numerical Solver

This study was performed with a bespoke conjugate thermal solver which includes models of both the internal cooling and the external film cooling layer. The solver has the facility to solve any cooling network of injection and ejection points for internal and external cooling flows. For the internal cooling flow, the solver takes account of heat transfer between the cooling flow and the wall, and of total pressure loss along the channels. These combined effects lead to complex coupling of heat and mass flows in the system because of the effects of: volume dilation (temperature and pressure change); changes in internal-channel Re and Nu; changes in channel total pressure loss; changes in cooling channel mass flow rate. The external film cooling is modelled using a control-volume-style entrainment-based model of a mixing layer. We describe these models in detail in this section.

Correlations for Internal Heat Transfer Coefficient. Local internal heat transfer coefficient, $h_c(x)$ depends on local temperature-dependent fluid properties, $h_c(x) = f(c_{pc}, k_c, u_c, \mu_c, \rho_c)$, where $c_{pc}(x)$, $k_c(x)$, $u_c(x)$, $\mu_c(x)$ and $\rho_c(x)$ are local values of specific heat capacity, thermal conductivity, channel velocity, dynamic viscosity and density of the internal coolant. We evaluate fluid properties at each cooling-channel location for each iteration step of the solution using the evaluated distribution of $T_{0c}(x)$ at the corresponding solution step. This allows pressure loss and internal heat transfer coefficients to be updated as the numerical solver is run to convergence. The choice of duct heights (H_{1c} for the reverse-pass cooling duct and H_{3c} for the TE slot) and cross-sectional areas of the film cooling row and TE slot (A_{1c} and A_{3c}, respectively) were chosen to be representative of typical cooling systems, and to—in conjunction with other BCs—give target values of surface-average cooling effectiveness ($\bar{\theta} = 0.5$) and coolant-to-mainstream mass flow rate ratios ($\dot{m}_{1c}/\dot{m}_{1h} = 0.079$ and $\dot{m}_{3c}/\dot{m}_{1h} = 0.019$).

We now consider the specific correlations used for cooling duct heat transfer coefficients and pressure loss.

We define the local cooling-channel Reynolds number by

$$\mathrm{Re}_c(x) = \frac{\rho_c(x) u_c(x) D(x)}{\mu_c(x)} \tag{12}$$

where $D(x)$ is hydraulic diameter of the duct. We differentiate between D_{1c} for the leading-circuit hydraulic diameter, and D_{3c} for the TE circuit hydraulic diameter. Local cooling-channel Prandtl number is defined by

$$\mathrm{Pr}_c(x) = \frac{c_{pc}(x)\mu_c(x)}{k_c(x)} \tag{13}$$

The local cooling-channel Nusselt number is then given by the Dittus-Boelter equation [15].

$$\mathrm{Nu}_c(x) = 0.023 \mathrm{Re}_c(x)^{0.8} \mathrm{Pr}_c(x)^{0.4} \tag{14}$$

Local cooling-channel heat transfer coefficient is then defined by

$$h_c(x) = \frac{\mathrm{Nu}_c(x) k_c(x)}{D(x)} \tag{15}$$

Correlation (14) was used for the TE-circuit flows of all three systems, and for the leading-circuit (reverse-pass) flows of system 1 and system 3. For the leading circuit of system 2, correlation (14) was augmented by applying a multiplication factor, $K(x)$

$$\mathrm{Nu}_c(x) = 0.023\, K(x) \mathrm{Re}_c(x)^{0.8} \mathrm{Pr}_c(x)^{0.4} \tag{16}$$

where $K(x)$ was set to give constant Nu *for the reference TR* (i.e. $\mathrm{Nu}_c/\mathrm{Nu}_c(0) = 1$ for $0 \le x/C_x < 0.75$) with the value set to that associated with the fluid conditions *at duct outlet*. The same distribution $K(x)$ was then used at non-reference TR, with terms $\mathrm{Re}_c^{0.8}(x)$ and $\mathrm{Pr}_c^{0.4}(x)$ being calculated based on local fluid properties and local velocity. This was an artificial way of setting constant Nu at the reference condition, with *physically meaningful variation with TR* away from the reference condition. For the distributed-inlet flow network of system 2, we are primarily interested in different coupling of the system (from system 1 and system 3) due to different mass flow rate distribution, and therefore any physically-based variation in the system serves our purpose.

Distributions $h_c(x)$ for all three systems are presented and discussed in the results section.

Correlations for Cooling Channel Pressure Loss. Friction coefficient, $f_c(x)$ was evaluated from the smooth-pipe Moody chart correlations (see, for example, [16]). For the leading circuit, total pressure gradient at position x, $\mathrm{d}p_{0c}(x)/\mathrm{d}x$, was evaluated using the *Moody friction factor equation*

$$\frac{\mathrm{d}p_{0c}(x)}{\mathrm{d}x} = \frac{4 f_c(x)}{D_{1c}} \frac{1}{2} u_c(x)^2 \tag{17}$$

where u_c is the local channel velocity given by

$$u_c(x) = \frac{\dot{m}_c(x)}{\rho_c(x) w H_{1c}} \tag{18}$$

where $\rho_c(x)$ is the local density of internal cooling flow and w is plate width. We use this correlation for systems 1–3.

Analysis of the TE circuit followed identical principles (hydraulic diameter D_{3c}; duct height H_{3c}).

Correlations for External Heat Transfer Coefficient. The local external heat transfer coefficient was evaluated using flat plate heat transfer correlations using the local fluid properties of the external mixing layer (we discuss this concept later). Local external Reynolds number is defined by

$$\mathrm{Re}_m(x) = \frac{\rho_m(x) u_m(x) x}{\mu_m(x)} \tag{19}$$

where $\rho_m(x)$ is the local density in the mixing layer, and $\mu_m(x)$ is the local dynamic viscosity. The local velocity of the mixing layer, $u_m(x)$, is that obtained when a flow of the mass-mean total pressure of the mixing layer is expanded isentropically to the static pressure set by an isentropic mainstream flow. Local external Prandtl number is defined by

$$\mathrm{Pr}_m(x) = \frac{c_{pm}(x)\mu_m(x)}{k_m(x)} \tag{20}$$

where $c_{pm}(x)$ is the local specific heat capacity at constant pressure in the mixing layer, and $k_m(x)$ is the local thermal conductivity.

For the Nusselt number distribution we use a flat plate correlation for turbulent flow [16]

$$\mathrm{Nu}_m(x) = 0.0296 \mathrm{Re}_m(x)^{4/5} \mathrm{Pr}_m(x)^{1/3} \tag{21}$$

Finally, the local external heat transfer coefficient is defined by

$$h_m(x) = \frac{\mathrm{Nu}_m(x) k_m(x)}{x} \tag{22}$$

The flat plate correlations give results of somewhat similar form to typical external heat transfer coefficient distributions for HPNGV pressure sides and suction sides (assuming the flow has fully transitioned in the showerhead region). They are considered sufficiently accurate for our purpose, namely predictions of *changes* in overall cooling effectiveness with TR, because they have sound physical basis (variation of h_m with Nu_m and Pr_m; dependence on local fluid properties; etc.) which allows physically-meaningful responses to changes in the system boundary conditions.

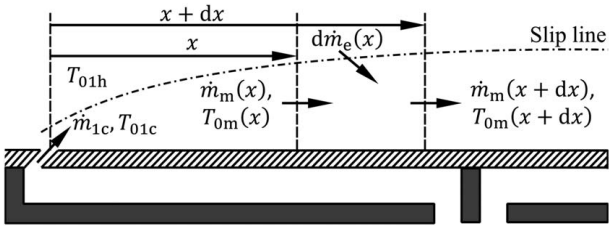

Fig. 4 Schematic illustration of the fully-mixed mixing layer

Distributions $h_m(x)$ for all three systems are presented and discussed in the results section.

Definition of the External Mixing Layer. We define an *external mixing layer* as the region adjacent to the wall in which the coolant ejected from the film cooling row mixes with hot gas. This is shown schematically in Fig. 4. We make the following assumptions about the behaviour of this layer:

(a) Static pressure, $p(x)$, is constant in the wall-normal direction. This means that the local static pressures in the mainstream and mixing layers are the same $p_m(x) = p_h(x) = p(x)$. Total pressures can be—slightly—different and the boundary may be considered as being represented by a *slip line*.
(b) The mixing layer is *fully mixed*, with a mass flow rate distribution for integrated entrained hot gas, $\dot{m}_e(x)$, that gives the desired mixing-layer *effectiveness distribution*, $\eta_{ML}(x)$, for the reference temperature ratio, TR = 2.0.

These assumptions allow calculation of the system static pressure distribution (from BCs, geometric area distribution, and simultaneous solution of both streams) and the mixing layer effectiveness distribution (from energy conservation, for entrainment subject to some similarity conditions we discuss later) for any conditions of TR. Real gas properties are considered in these calculations. Though the assumption of the fully-mixed layer differs significantly from the physical situation of temperature gradient within the near-wall layer, by arbitrarily setting the entrainment rate to match the desired effectiveness distribution for the reference condition, and because there is sound physical basis for the way *changes* from this condition are calculated, we believe it to be a useful proxy-model for the particular purpose of evaluating changes in overall effectiveness with temperature ratio. Another example of the use of an assumed fully-mixed mixing layer is that of Kirollos and Povey [17], who use it for the purpose of film superposition calculations. In [17], although individual mixing-layers take—by definition—the arbitrary thicknesses that satisfy the required single-film-cooling-row effectiveness distributions, the superposed solution is accurate. The point is that whilst layer thickness is arbitrary, much of the remaining physics is accurate.

We discuss the methods for evaluating pressure distribution and effectiveness distribution in the next section.

Effectiveness Distribution of the Mixing Layer. We define effectiveness of the mixing layer at the reference temperature ratio, $\eta_{ML}^{TR=2.0}(x)$, based on a typical incompressible adiabatic film effectiveness correlation (Vinton et al. [18]) for a single row of cooling holes

$$\eta_{aw}(x) = 0.4e^{-1.4x/C_x} \tag{23}$$

Now recall Eq. (3)

$$\eta_{ML}(x) = \frac{c_h(x)T_{01h} - c_m(x)T_{0m}(x)}{c_h(x)T_{01h} - c_c(x)T_{02c}}$$

where each term has an individual recovery ratio distribution ($c_h(x)$, $c_m(x)$ and $c_c(x)$) so as to constrain values of η_{ML} to the range $0 < \eta_{ML} < 1$. For the case of TR = 2.0, we equate Eqs. (23) and (3) giving

$$\eta_{ML}^{TR=2.0}(x) = \eta_{aw}(x) \tag{24}$$

which defines $T_{0m}^{TR=2.0}(x)$ by rearrangement of terms. The resulting integrated entrainment rate distribution, $\dot{m}_e^{TR=2.0}(x)$, is that which satisfies conservation of mass and energy (full equation not shown).

For *non-reference* temperature-ratio we assume that the integrated entrained hot gas mass flow rate, $\dot{m}_e(x)$, follows a geometric similarity argument as follows

$$\frac{\dot{m}_e(x)}{\dot{m}_{1h}} = \frac{\dot{m}_e^{TR=2.0}(x)}{\dot{m}_{1h}^{TR=2.0}} \tag{25}$$

That is, the *depth of the mixing layer* does not change with TR. In our situation of essentially-constant momentum flux ratio with TR, and essentially-constant external-side Mach number distribution with TR, the constraint Eq. (25) can be thought of as a similarity condition for the mixing-determining structures (for example, the penetration depth of the film and the turbulence length scale). Once $\dot{m}_e(x)$ is determined from Eq. (25), the total temperature of the mixing layer can be calculated by mass balance

$$T_{0m}(x) = \frac{\dot{m}_{1c}c_{p1c}T_{01c} + \dot{m}_e(x)c_{p01h}T_{01h}}{\dot{m}_m(x)c_{p0m}(x)} - \frac{w\int_0^x \dot{q}_m dx}{\dot{m}_m(x)c_{p0m}(x)} \tag{26}$$

where c_{p1c} is specific heat capacity of cooling flow at plane 1, c_{p01h} is specific heat capacity of the mainstream flow at corresponding temperature T_{01h}, $w\int_0^x \dot{q}_m dx$ is the integrated (between 0 and x) external convective heat flux, and $c_{p0m}(x)$ is specific heat capacity of the mixing layer evaluated at corresponding temperature T_{0m}. Equation (26) defines both the driving temperature for heat transfer, $c_m(x)$ $T_{0m}(x)$, and the effectiveness of the mixing layer, $\eta_{ML}(x)$ (from Eq. (3)).

Distributions $\eta_{ML}(x)$ for all three systems are presented and discussed in the results section.

Calculation of External Static Pressure Distribution and Mainstream and Coolant Mass Flow Rate. In this section we describe how we simultaneously calculate the external static pressure distribution, $p(x)$, and the mainstream and (forward-circuit) coolant mass flow rates, $\dot{m}_h(x)$ and $\dot{m}_{1c}$.

The static pressure distribution sets the static pressure at the exit of the film cooling row (and therefore the cooling flow rate). The static pressure distribution varies slightly with TR, due to changes in, for example, specific heat capacities with temperature, causing changes in the local external Mach number distribution even for fixed domain-global PR.

In our model, the cross-sectional area of the mainstream (representing the vane), $A(x)$ varies linearly from inlet to exit as shown in Fig. 5. Domain-global BCs are set (either fixed exit Re and PR, or fixed PR with fixed exit pressure), which define the mainstream flow total pressure. The mainstream total temperature is defined by the given TR condition being studied. The coolant feed total pressure is defined by the coolant-to-mainstream pressure ratio.

We solve simultaneously and iteratively (to convergence) for mass flows and pressure distributions subject to the following constraints:

(i) Inlet total pressures, p_{01h} and p_{02c}, and domain-exit static pressure, p_3, defined by the domain-global and cooling-system BCs (see Fig. 1 and Table 1).
(ii) Cooling flow total temperature $T_{02c} = 300$ K, with mainstream total temperature, T_{01h} defined by the TR under consideration.
(iii) Distributions of local areas of mainstream flow and mixing layer flow, $A_h(x)$ and $A_m(x)$, subject to the geometrical

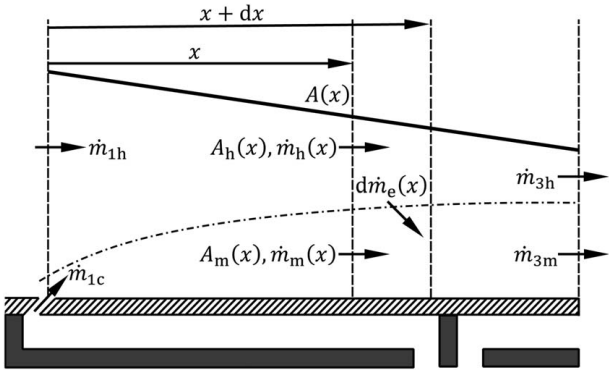

Fig. 5 Schematic of the mixing layer, showing boundary conditions on the mixing process

constraint $A_h(x) + A_m(x) = A(x)$ i.e. the two stream areas sum to the local passage area. This is illustrated in Fig. 5.

(iv) Adiabatic mainstream flow, $T_{0h}(x) = T_{01h}$, with no loss of total pressure, $p_{0h}(x) = p_{01h}$.

(v) Total pressure of the mixing layer defined by a simple mass average

$$p_{0m}(x) = \frac{\dot{m}_{1c} p_{01c} + \dot{m}_e(x) p_{01h}}{\dot{m}_m(x)} \tag{27}$$

where we note that the inlet total pressures p_{01h} and p_{02c} differ by only 2.5%, and that most of the entrainment happens at low Mach number ($M < 0.60$) limiting the impact of weaknesses in this model especially so far as changes with TR conditions are concerned.

(vi) Total temperature distribution of the mixing layer *for the reference TR*, $T_{0m}^{TR=2.0}(x)$, prescribed by Eq. (23) and equality with Eq. (24), which defines a particular associated integrated entrainment rate, $\dot{m}_e(x)$.

(vii) For the non-reference TR, we impose a geometric similarity condition on the mixing layer (see Eq. (25)) which is equivalent to the depth of the mixing layer being unchanged with TR. This allows $\dot{m}_e(x)$ and therefore $T_{0m}(x)$ to be calculated for any non-reference TR.

(viii) Mass and energy conservation in each cell, including through-wall heat fluxes.

(ix) The mixing layer boundary acts as a slip line, such that the static pressure either side is constant i.e. $p_h(x) = p_m(x) = p(x)$.

Temperature-dependent fluid properties are used in the analysis, and the (reverse-pass) forward-circuit mass flow rate, $\dot{m}_{1c}$, and associated channel exit total pressure, p_{01c}, are allowed to vary with external static pressure. For the case of the domain-global fixed PR BCs, these effects cause the coolant-to-mainstream mass flow rate ratio to change by approximately −21% as TR is varied between 2.0 to 1.2. The corresponding value for the domain-global fixed Re BC is −22%. The primary cause of this effect is a reduction in coolant mass flow rate as TR is decreased (approximately constant coolant momentum flux as coolant density decreases with increasing coolant temperature, leading to a reduction in coolant mass flow rate per unit area).

Discretisation Scheme for Numerical Solver. For each elemental cell in the mixing layer and internal cooling duct, we satisfy mass and energy conservation, taking account of convection heat transfer with the walls, and advection terms into and out of an elemental cell. On the external surface the driving temperature difference is taken to be $c_m(x)T_{0m}(x) - T_{w1}(x)$, i.e. we consider the recovery factor of the mixing layer to account for compressible flow effects. For the wall we consider energy conservation in the through-wall direction. Lateral conduction terms are omitted but can be shown to be very small (length ratio, $C_x/t_w = 100$) in comparison to through-wall terms. The solution was iterated to convergence, defined by the maximum residual in any heat flux term being less than 0.1% of the mean through-wall heat flux. This threshold was typically passed after 3 global iteration steps. A grid independence study was performed and the solution was found to be independent of mesh size for $dx \le 0.1$ mm and $dy \le 0.5$ mm. The final mesh had 10 cells in the through-wall direction and approximately 1×10^3 cells in the flow-wise direction.

Results I: Baseline Local Surface Boundary Conditions and Overall Cooling Effectiveness Distributions

In this section we present baseline (i.e. for reference TR = 2.0) local surface boundary conditions and overall cooling effectiveness results for the three cooling system networks (see Fig. 3). These form the reference case for all comparisons later in this paper, as we vary temperature ratio away from the reference TR. The reference TR domain-global and cooling system BCs are summarised in Table 1.

First, consider the resulting *local surface BCs* which are presented in Fig. 6 for all three cooling systems. Here we plot distributions of five parameters: effectiveness of the mixing layer, η_{ML}; local through-wall-average wall thermal conductivity, $\bar{k}_w$; external heat transfer coefficient, h_m; internal heat transfer coefficient, h_c; and internal cooling effectiveness, λ. Because we are primarily interested in the characteristic trends, and in differences between the three systems, absolute values are normalised by particular local values for system 1. For η_{ML}, h_m and $\bar{k}_w$, we normalise by values at the leading edge of the plate ($x/C_x = 0$) for which numerical values are: $\eta_{ML} = 0.40$, $h_m = 1720\,\mathrm{W\,m^{-2}K^{-1}}$, and $\bar{k}_w = 11.2\,\mathrm{W\,m^{-1}K^{-1}}$. For h_c and λ we normalise by values at the entrance to the reverse-pass cooling duct ($x/C_x = 0.75$) for which numerical values are: $h_c = 408\,\mathrm{W\,m^{-2}K^{-1}}$ and $\lambda = 0.994$ (small difference from unity arises due to recovery ratios).

Consider first the effectiveness distributions for the mixing layer, $\eta_{ML}(x)$. The trend is for exponential decay, in line with Eq. (23). Trends for all three cooling system networks are identical because the distribution is imposed at the reference TR.

Now consider the trend in external heat transfer coefficient, $h_m(x)$. The general trend is similar to $1/x$ in the region $0 \le x/C_x < 0.4$ due to the $1/x$ term in Eq. (22). In the region $0.4 \le x/C_x < 1$,

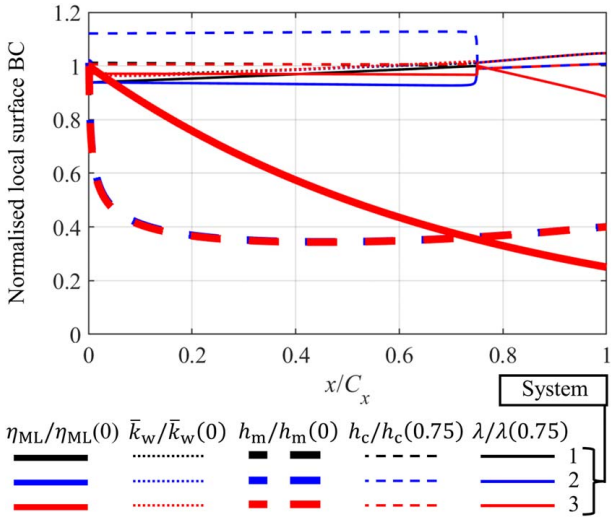

Fig. 6 Local surface BCs for cooling system networks 1–3 at the reference TR. Absolute values are normalised by particular local values for system 1 (values at $x/C_x = 0$ for η_{ML}, $\bar{k}_w$, and h_m; values at $x/C_x = 0.75$ for h_c and λ).

$h_m(x)$ monotonically increases because the rate at which $1/x$ term decays is smaller than the rate of increase of local external Reynolds number, $Re_m(x)$, due to increasing local external velocity, $u_m(x)$. The trends are almost identical for all three cooling system networks with second-order differences due to, for example: differences in cooling mass flow rate due to differences in pressure loss from inlet to exit of the reverse-pass cooling duct; differences in through-wall heat flux distributions between the three systems caused by slight differences in mixing layer temperature.

The local through-wall-average wall thermal conductivity, $\bar{k}_w(x)$, is approximately constant with surface distance, with RMS variation from the surface-averaged value of 0.26 W m^{-1} K^{-1} and maximum variation of 0.56 W m^{-1} K^{-1}. These are equivalent to 2.3% and 5.0% of the surface-averaged value, respectively.

Now consider the internal heat transfer coefficient distribution, $h_c(x)$. The trends for the TE circuit ($0.75 \le x/C_x < 1$) are identical for all three cooling system networks: this is expected because this is a common part of the networks. Small differences in this region are caused by velocity variation along the channel. The values in the region of the leading circuit ($0 \le x/C_x < 0.75$) are approximately constant, with a mean value approximately 8.8% higher for system 2 (difference in the way the distributed-inlet boundary condition was set).

Finally, consider the internal cooling effectiveness distributions, $\lambda(x)$. In the TE circuit ($0.75 \le x/C_x < 1$), for all three cooling systems, $\lambda(x)$ starts from a value of 0.99 at $x/C_x = 0.75$ and falls approximately linearly to a value of approximately 0.88 at $x/C_x = 1.00$, as heat is picked up in the channel. In the region of the leading circuit, the trend for system 1 is approximately linear decay between values of 0.99 ($x/C_x = 0.75$) and 0.93 ($x/C_x = 0$) as heat is picked up in the reverse-pass channel. In system 2 (distributed inlet) the fluid temperature is always much closer to the inner wall temperature (lower initial mass flow; incremental addition of coolant) and $\lambda(x)$ is in the range $0.921 < \lambda(x) < 0.932$ (i.e. approximately constant) in the region $0 \le x/C_x < 0.75$ (i.e. the entire passage from a very short distance downstream of the inlet). For system 3, the cooling flow is fully-mixed by definition and $\lambda(x)$ takes the constant value 0.96.

Resulting overall cooling effectiveness distributions, $\theta(x)$, for all three cooling system networks at the reference TR are presented in Fig. 7. Distributions were similar for all three cooling system networks, with values being bounded by $0.38 < \theta(x) < 0.58$, and with mean values $\bar{\theta} = 0.500$, 0.502 and 0.500, for cooling system networks 1–3 respectively. Mean RMS difference between trends was 0.004, and maximum difference 0.023. It is interesting that the resulting trends are so insensitive to fairly large changes in the network of the design. We now describe the physical basis for the underlying trends in more detail.

The sudden increase in $\theta(x)$ between $x/C_x = 0$ and $x/C_x = 0.08$ is driven by a steep reduction in external heat transfer coefficient (see Fig. 6) near the leading edge as the boundary layer thickens. For $x/C_x > 0.08$, the trend in θ is an approximately-linear decrease from a peak at 0.57 to a minimum of 0.39. In this region the external heat transfer coefficient is approximately constant, and the trend in θ is primarily caused by an approximately linear reduction in the mixing layer effectiveness, η_{ML}.

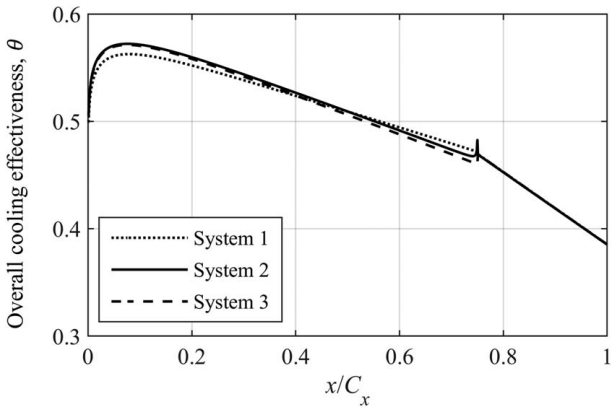

Fig. 7 Overall cooling effectiveness distributions, $\theta(x)$, for cooling system networks 1–3 at the reference TR

Results II: Effect of Temperature Ratio on Overall Cooling Effectiveness

In this section we consider the effect of temperature ratio on overall cooling effectiveness. Results are presented for system 1 for domain-global boundary conditions of fixed PR. We show later that the result is almost completely independent of the cooling system network for the types of network considered. We also show that the *overall* change in overall cooling effectiveness (sum of effects associated with changes in each of five local surface BCs) is relatively independent of the domain-global boundary conditions, despite significant changes associated with individual local surface BCs for the domain-global BC of fixed exit Re with fixed PR.

Predictions were performed over the TR range $1.2 \le TR \le 2.0$ for fixed p_{01h}, p_{02c}, p_{3h}, CMPR and T_{02c}. The changes in overall cooling effectiveness distribution from that for the reference TR (Fig. 7), $\Delta\theta = \theta - \theta^{TR=2.0}$ are presented in Fig. 8. The effect of reducing TR from the reference condition is to reduce effectiveness. This effect occurs primarily because of a reduction in the heat capacity flow rate ratio ($\dot{m}_{1c}c_{p1c}/\dot{m}_{1h}c_{p01h}$) as TR is reduced, causing a reduction in the mixing layer effectiveness. We discuss this effect, and other second-order effects, in detail in the following sections. The surface-mean change in overall cooling effectiveness from the value for the reference TR, $\overline{\Delta\theta}$, was −0.007, −0.015, −0.026 and −0.041 for TRs 1.8, 1.6, 1.4 and 1.2 respectively. As percentages of the target mean effectiveness ($\bar{\theta} = 0.500$) these are equivalent to changes of −1.40%, −3.00%, −5.20% and −8.20% respectively. This is the key result of this paper, and remaining sections are largely dedicated to robustly examining this result, and looking at the range of boundary conditions for which it is valid.

For typical mainstream and coolant temperatures [19] of 1750 K and 875 K, and based on our preferred definition of overall effectiveness (Eq. (2)), if tests were run at typical laboratory conditions with TR = 1.2, and results were not corrected to engine conditions, scaled uncorrected results would be higher than true engine metal temperatures by 35.9 K. That is, tests at typical laboratory temperatures overestimate component temperature based on simple scaling.

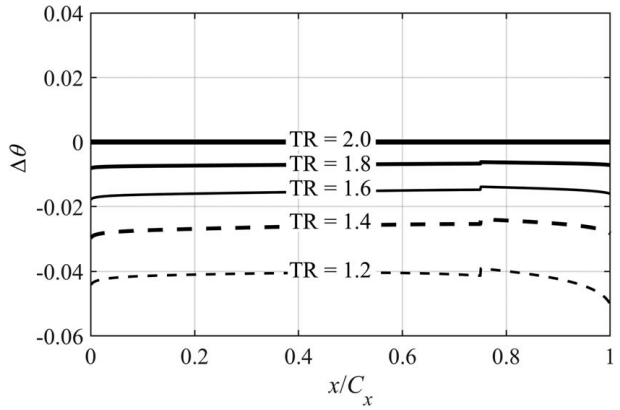

Fig. 8 Distributions of change in overall cooling effectiveness, $\Delta\theta(x)$, as a function of normalised surface distance, x/C_x, for temperature ratios in the range $1.2 \le TR \le 2.0$. Results are for system 1 for domain-global boundary conditions of fixed PR.

So far as the trends with surface distance are concerned, we see (Fig. 8) that the change is approximately constant with surface distance in the region of the leading circuit (maximum ratio of 1.09), and vary by a factor of about 1.3 in the region of the trailing circuit.

For the case of the fixed PR domain-global BC this is explained by a combination of three effects. Firstly (see Fig. 6) $\eta_{ML}(x)$ is significantly larger at the leading edge (value of approximately 0.40) than the trailing edge (value of approximately 0.10), which, when combined with the geometric similarity mixing constraint—Eq. (25)—means greater change with TR in *absolute* values of $\eta_{ML}(x)$ at the leading rather than the trailing edge: that is, the absolute reduction in $\eta_{ML}(x)$ as TR is reduced is greater at the LE than the TE. The second effect is an increase in the external heat transfer coefficient as TR is reduced (due to an increase in local external Reynolds number with decreasing mainstream temperature), which acts to further decrease the overall cooling effectiveness. The trend for the second effect is an increase in magnitude with surface distance in the region of the leading circuit but at a lower rate than the first effect. This is explained as follows: the change in $h_m(x)$ with TR, $\Delta h_m(x)$, is approximately constant with surface distance and the sensitivity of $\theta(x)$ to changes in $h_m(x)$ increases with surface distance due to an increase in the magnitude of $\lambda(x) - \eta_{ML}(x)$ caused by an increase in $\lambda(x)$ and a reduction in $\eta_{ML}(x)$ as we move from the leading edge $(x/C_x = 0)$ to plane 2 $(x/C_x = 0.75)$. This can be understood by considering the partial derivative of Eq. (11) with respect to h_m. In the region of the trailing edge circuit the magnitude of the second effect decreases with surface distance. This can be explained as follows: sensitivity of $\theta(x)$ to changes in $h_m(x)$ decreases with surface distance due to a reduction in the magnitude of $\lambda(x) - \eta_{ML}(x)$ due to a combination of a reduction in $\lambda(x)$ and a (small) reduction in $\eta_{ML}(x)$ as we move from plane 2 $(x/C_x = 0.75)$ to the trailing edge plane 3 $(x/C_x = 1)$. The third effect is a reduction in internal cooling effectiveness as TR is reduced, which acts to further decrease the overall cooling effectiveness. We explain this effect as follows. The effect of compressibility in the system results in recovery ratios less than unity and, for temperature ratios greater than unity, this has the effect of reducing λ (compared to the case $c_c(x) = c_h(x) = c_m(x) = 1$). The effect of decreasing TR from TR = 2.0 is to amplify the magnitude of the reduction in λ caused by this compressibility effect.

In combination, and taking into account two other second-order effects (see later sections), these effects lead to the trends of Fig. 8. Although this is to some extent a system-specific result, the characteristic trend is typical of most HPNGVs.

We will see in later sections that the *overall* result of Fig. 8 is insensitive to the choice of domain-global BCs (fixed PR alone, or fixed exit Reynolds number and fixed PR), but the *contributions* from individual local surface BCs are very different for different domain-global BCs.

Results III: Decomposed Contributions From Changes in Local Surface Boundary Conditions

In this section we decompose the overall change in θ with TR into the effects associated with changes in five local surface BCs. We choose the following local surface boundary conditions for this process: effectiveness of the mixing layer, η_{ML}; local through-wall-average wall thermal conductivity, $\bar{k}_w$; external heat transfer coefficient, h_m; internal heat transfer coefficient, h_c; and internal cooling effectiveness, λ. That is, $\theta = f(\eta_{ML}, \bar{k}_w, h_m, h_c, \lambda)$. Though somewhat arbitrary, we justify this choice of variables with the weak analytical argument that for a simple zero-dimensional model these five parameters are sufficient to define the surface temperature. This argument has been presented. We refer to the effects associated with each of these five boundary conditions as effect 1 to effect 5. In the analysis that follows, where we can ascribe changes in any particular one of these local surface boundary condition to changes in underlying parameters, we do so. A schematic diagram of the cooling system network showing the region which each effect (1 to 5) is associated with, is shown in Fig. 9.

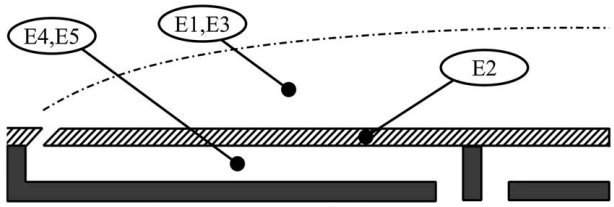

Fig. 9 Schematic of the cooling system showing the regions with which each of the effects 1–5 are most associated

Our results will be presented for system 1 for fixed PR boundary conditions. We show later that the general result is insensitive to overall system boundary conditions (fixed PR or fixed exit Re with fixed PR) and insensitive to the internal cooling system network.

To perform these predictions, we do the following:

(i) We converge solutions at each of five TR conditions corresponding to TR = 2.0, 1.8, 1.6, 1.4 and 1.2. In these simulations all fluid properties and local BCs are for the domain-global and cooling system BCs presented in Table 1. These predictions represent the natural converged state of the system at a given TR condition.

(ii) From each of the five converged simulations (at five TR conditions) we extract distributions of overall cooling effectiveness, $\theta(x)$, and distributions of each of the five local surface BCs: $\eta_{ML}(x)$, $\bar{k}_w(x)$, $h_m(x)$, $h_c(x)$ and $\lambda(x)$. The result is $5 \times 6 = 30$ distributions. The structure of this data is shown in Fig. 10 (only average values of the underlying distributions presented).

(iii) The surface-mean change in the value of $\theta(x)$ with TR, $\overline{\Delta\theta}$, represents the sensitivity of overall cooling effectiveness to TR when all variables are allowed to vary *in a natural co-dependent way* with TR. This has been discussed in the context of Fig. 8.

Fully converged simulations at five TRs

TR	$\bar{\theta}$ (–)	$\bar{\eta}_{ML}$ (–)	$\bar{k}_w$ (W m^{-1} K^{-1})	$\bar{h}_m$ (W m^{-2} K^{-1})	$\bar{h}_c$ (W m^{-2} K^{-1})	$\bar{\lambda}$ (–)
2.0	0.5000	0.2164	11.17	646.7	409.5	0.9558
1.8	0.4930	0.2108	10.64	659.1	411.4	0.9542
1.6	0.4846	0.2041	10.10	673.1	413.2	0.9518
1.4	0.4740	0.1962	9.54	689.3	415.1	0.9472
1.2	0.4587	0.1866	8.97	708.4	417.0	0.9344

Effect 1: resulting value of $\bar{\theta}'$ when only η_{ML} is perturbed

$\bar{\theta}'$ (–)
0.5000
0.4965
0.4924
0.4874
0.4815

Fig. 10 Schematic of data structure used in the process for predicting changes in overall cooling effectiveness when one local surface BC is changed—in isolation of other local surface BCs—from its value at reference TR. Example for effect 1.

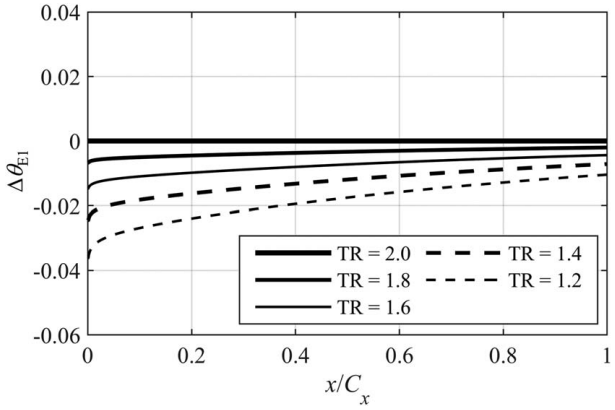

Fig. 11 Change in overall cooling effectiveness when the effectiveness of the mixing layer, η_{ML}, is changed—in isolation of other local surface BCs—from its value at reference TR

(iv) To perform a simple decomposition of contributions associated with changes in each of the five local surface BCs ($\eta_{ML}(x)$, $\bar{k}_w(x)$, $h_m(x)$, $h_c(x)$, $\lambda(x)$), treating each local surface BC in turn, we take the converged simulation at the reference temperature ratio, and impose conditions of a *single particular local surface BC from converged simulations at all other non-reference TRs*. We then compare the resulting distributions $\theta'(x)$ to the original distributions $\theta(x)$. The difference, $\Delta\theta(x) = \theta'(x) - \theta(x)$, is taken to be due to the single variable that was perturbed. Later, we use a check-sum approach to test the extent of validity of this implicit linear superposition assumption. A schematic of the data that is used in this process is shown in Fig. 10 for effect 1, changes in $\eta_{ML}(x)$.

We now consider each of the effects in turn. All the analysis that follows is for system 1, for the fixed PR domain-global BC.

Effect 1: Changes in Overall Cooling Effectiveness due to Changes in Effectiveness of the Mixing Layer. We now consider the effect on θ of varying the effectiveness of the mixing layer (η_{ML}) —in isolation of other local surface BCs—from its value at the reference TR. We change the distributions $\eta_{ML}(x)$ to the values they take at TRs in the range $1.2 \le TR \le 2.0$, whilst keeping all other local surface BCs ($\bar{k}_w$, h_m, h_c and λ) equal to the values they take in a converged simulation at the reference TR. If linear superposition can be assumed to be valid, this allows us to determine the impact on θ of changes in η_{ML} (with TR) for fixed conditions of other local surface BCs. We refer to these changes as $\Delta\theta_{E1}(x)$, where the sign convention is $\Delta\theta_{E1}(x) = \theta(x) - \theta(x)^{TR=2.0}$. The changes $\Delta\theta_{E1}(x)$ are plotted for the range $1.2 \le TR \le 2.0$ in Fig. 11.

The effect of reducing TR from the reference condition is to reduce the effectiveness of the mixing layer, which decreases θ due to higher non-dimensional driving external temperature. This effect occurs primarily because of a reduction in the heat capacity flow rate ratio ($\dot{m}_{1c}c_{p1c}/\dot{m}_{1h}c_{p01h}$) as TR is reduced, causing a reduction in the mixing layer effectiveness. The surface-mean changes in overall cooling effectiveness from the value for the reference TR, $\overline{\Delta\theta}_{E1}$ were −0.004, −0.008, −0.013, and −0.019 for TRs 1.8, 1.6, 1.4 and 1.2 respectively. As percentages of the target mean effectiveness ($\overline{\theta} = 0.500$) these are equivalent to changes of −0.80%, −1.60%, −2.60% and −3.80% respectively.

So far as the trends with surface distance are concerned, we see (Fig. 11) that the change, $\Delta\theta_{E1}(x)$, is greater at the leading edge ($x/C_x = 0$) than the trailing edge ($x/C_x = 1.0$) by a factor of approximately 3.4. This is because (see also discussion in context of Fig. 8) $\eta_{ML}(x)$ takes greater absolute values near the leading edge (see Fig. 6) which when combined with the geometric similarity condition for mixing (Eq. (25)), means greater *absolute* change in $\eta_{ML}(x)$ near the leading edge compared with the trailing edge. The underlying physical effect is that when TR is reduced from the reference condition, a relative increase in hot-gas mass flow rate (due to increase in density that outweighs the reduction in velocity) reduces the coolant-to-mainstream mass flux ratio, reducing the effectiveness of the mixing layer.

To provide insight into second-order effects, we now perform a sensitivity analysis of all influences on $\eta_{ML}(x)$ as TR is varied. The full equation for effectiveness of the mixing layer (not shown) arises from consideration of mass and energy conservation within the mixing layer and has the functional relationship $\eta_{ML} = f(\dot{m}_e, \dot{m}_{1c}, c_{p01h}, c_{p1c}, \varepsilon, \dot{m}_{3c}, c_c, c_h, c_m, c_{p2c}, T_{02c}, T_{01h})$. In this equation, the recovery ratios $c_h(x)$, $c_m(x)$ and $c_c(x)$ are approximately equal to unity (minimum value 0.98), and vary little with temperature ratio. Taking the approximation $c_h(x) = c_m(x) = c_c(x) = 1$, and taking the further approximation of constant specific heat capacity of the coolant within the leading circuit (i.e. $c_{p1c} = c_{p2c}$; true to within 0.10%) we can reduce the more complex functional relationship to the form

$$\eta_{ML}(x) = \frac{1 - \varepsilon(x)\left(1 + \dfrac{\dot{m}_{3c}}{\dot{m}_{1c}}\right)}{1 + \left(\dfrac{\dot{m}_e(x)}{\dot{m}_{1c}}\right)\left(\dfrac{c_{p01h}}{c_{p1c}}\right)} \tag{28}$$

where $\dot{m}_e(x)/\dot{m}_{1c}$ is the ratio of integrated (between 0 and x) entrainment mass flow rate to coolant mass flow rate at plane 1, $\dot{m}_{3c}/\dot{m}_{1c}$ is the ratio of trailing circuit to leading circuit coolant mass flow rate, c_{p01h}/c_{p1c} is the specific heat capacity ratio, and $\varepsilon(x)$ is the total non-dimensional external-side heat flux between any location x and the cooling channel inlet ($x/C_x = 0.75$) i.e.

$$\varepsilon(x) = \frac{w\int_x^{x/C_x=0.75} \dot{q}_m dx}{(\dot{m}_{1c} + \dot{m}_{3c})c_{p2c}(T_{01h} - T_{02c})} \tag{29}$$

where we have normalised by the maximum heat pick up of the combined coolant streams (streams heated from T_{02c} to T_{01h}), taking the assumption of constant specific heat capacity for coolant flow within the ducts.

In Eq. (28) we express η_{ML} as a function of four non-dimensional groups, i.e. $\eta_{ML} = f(\dot{m}_e(x)/\dot{m}_{1c},\ \dot{m}_{3c}/\dot{m}_{1c},\ c_{p01h}/c_{p1c},\ \varepsilon')$. We evaluate the sensitivity of surface-averaged effectiveness, $\bar{\eta}_{ML}$, to each of the four non-dimensional groups by partial derivative of Eq. (28) with respect to each in turn. We consider the sensitivity of the *surface-averaged* effectiveness, $\bar{\eta}_{ML}$, to each group in order to give insight into the physical mechanisms that drive changes in $\eta_{ML}(x)$. Percentage contributions of each non-dimensional group to the overall change in surface-average film effectiveness ($\Delta\bar{\eta}_{ML}$) are presented as a bar chart in Fig. 12. We recall that moving from the reference TR to lower-than-reference TR causes a reduction in $\bar{\eta}_{ML}$, which causes a reduction in θ (negative value of $\Delta\theta_{E1}$). We see from Fig. 12 that this effect is dominated by the increase in the ratio of integrated entrained hot gas to coolant mass flow rate ($\dot{m}_e/\dot{m}_{1c}$), which is driven by reduction in coolant-to-mainstream density ratio (ρ_{1c}/ρ_{1h}) due to an increase in ρ_{1h} as TR is reduced (an effect that outweighs the decrease in mass flow with decreasing mainstream velocity with reducing TR). The magnitude of this effect is 117% of the overall change, and is offset by a 0.03% contribution associated with the change in $\dot{m}_{3c}/\dot{m}_{1c}$, a −17.4% contribution associated with the change in c_{p01h}/c_{p1c}, and a 0.42% contribution associated with the change in ε'. In summary, it is the change in the ratio of integrated entrained hot gas to coolant mass flow rate and the change in heat capacity ratio that dominate the change in $\bar{\eta}_{ML}$ that gives rise to a change in θ. We note that the product of $\dot{m}_e(x)/\dot{m}_{1c}$ and c_{p01h}/c_{p1c} is the ratio of the heat capacity flow rates of the coolant and entrained hot gas ($\dot{m}_{1c}c_{p1c}/\dot{m}_e(x)c_{p01h}$). Due to the geometric similarity condition for mixing (Eq. (25)), this is directly proportional to the

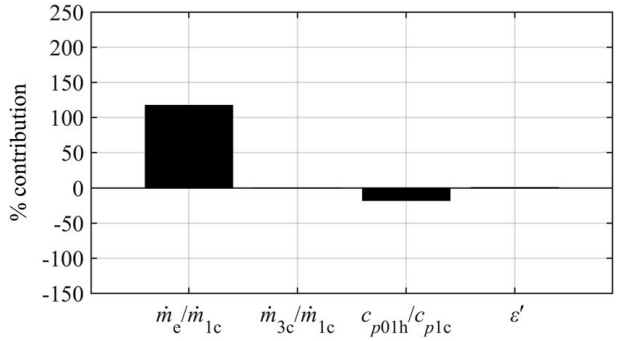

Fig. 12 Percentage contributions of three underlying terms to changes in surface-averaged effectiveness of the mixing layer, $\bar{\eta}_{ML}$

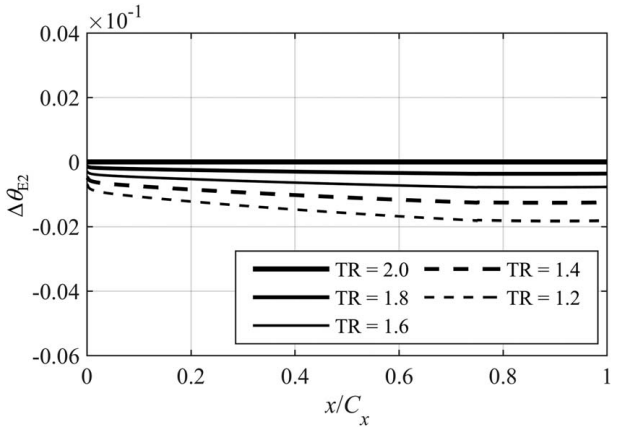

Fig. 13 Change in overall cooling effectiveness when the local through-wall-average wall thermal conductivity, $\bar{k}_w$, is changed —in isolation of other local surface BCs—from its value at reference TR

coolant-to-mainstream heat capacity flow rate ratio ($\dot{m}_{1h}c_{p01h}/\dot{m}_{1c}c_{p1c}$), which is the primary variable responsible for determining the mixing layer effectiveness (see Ornano and Povey [1]). From a dimensional-analysis standpoint this combined parameter is of predominant importance in this problem. Here we treat the two underlying terms separately, however, to identify that the root cause of the change in coolant-to-mainstream heat capacity flow rate ratio is almost primarily related to the change in mass flow rate ratio and only secondarily dependent on the heat capacity ratio.

In summary, as we move from the reference TR to lower-than-reference TR, η_{ML} decreases, primarily due to a decrease in the ratio of integrated entrained hot gas and the coolant mass flow rate. The decrease in η_{ML} leads to a decrease in θ.

Effect 2: Changes in Overall Cooling Effectiveness due to Changes in Local Through-Wall-Average Wall Thermal Conductivity. We now consider the effect on θ of varying local through-wall-average (in y-direction) wall thermal conductivity ($\bar{k}_w$)—in isolation of other local surface BCs—from its value at the reference TR. As described in the previous section, we change the distributions $\bar{k}_w(x)$ to the values they take at TRs in the range $1.2 \le TR \le 2.0$, whilst keeping all other local surface BCs (η_{ML}, h_m, h_c and λ) equal to the values they take in a converged simulation at the reference TR. If linear superposition can be assumed to be valid, this allows us to determine the impact on θ of changes in $\bar{k}_w$ for fixed conditions of other local surface BCs. We refer to these changes as $\Delta\theta_{E2}(x)$, where the sign convention is $\Delta\theta_{E2}(x) = \theta(x) - \theta(x)^{TR=2.0}$. The changes $\Delta\theta_{E2}(x)$ are plotted for the range $1.2 \le TR \le 2.0$ in Fig. 13.

The effect of reducing TR from the reference condition is to decrease wall thermal conductivity, which reduces θ due to higher Biot number (less coupling of internal and external wall, so lower effect of internal cooling). Here we take the correlations $k_w = 2.7 + 0.019T_w$ which is typical for nickel alloy [20]; that is, a weak positive linear trend between k_w and T_w. The surface-mean changes in overall cooling effectiveness from the value for the reference TR, $\overline{\Delta\theta}_{E2}$ were −0.0003, −0.0007, −0.0011, and −0.0015 for TRs 1.8, 1.6, 1.4 and 1.2 respectively. As percentages of the target mean effectiveness ($\bar{\theta} = 0.500$) these are equivalent to changes of −0.06%, −0.14%, −0.22% and −0.30% respectively. We see that this effect is small in the temperature range dictated by our domain-global BCs. We revisit this point in the context of engine-like absolute temperatures in a later section.

So far as the trends with surface distance are concerned, we see (Fig. 13) that the change, $\Delta\theta_{E2}(x)$, is greater at the trailing edge ($x/C_x = 1.0$) than the leading edge ($x/C_x = 0$) by a factor of approximately 2.4. We now explain this effect. As we reduce TR, the absolute change in through-wall-average thermal conductivity, $\Delta\bar{k}_w$, is larger at the trailing edge than the leading edge because the absolute change in wall temperature with TR, ΔT_w, is larger at the trailing edge than the leading edge. This is because the absolute wall temperature, T_w is greater at the trailing edge, which results from the effectiveness of the mixing layer, $\eta_{ML}(x)$, decaying with axial distance (see discussion in the context of Fig. 6). The greater decrease, $\Delta\bar{k}_w$ (recall this term takes negative value with decreasing TR) at the TE, leads to a greater increase in Biot number than at the leading edge, leading to greater change $\Delta\theta_{E2}$ at the trailing edge.

In summary, as we move from the reference TR to lower-than-reference TR, $\bar{k}_w$ decreases, due to a decrease in T_w. This leads to a decrease in θ because of an attendant increase in Biot number, which has the effect of reducing the impact of internal cooling on the external temperature (acts to decouple the surfaces). The effect is quite small in comparison to other effects.

Effect 3: Changes in Overall Cooling Effectiveness due to Changes in External Heat Transfer Coefficient. We now consider the effect on θ of varying external heat transfer coefficient (h_m)—in isolation of other local surface BCs—from its value at the reference TR. We change the distributions $h_m(x)$ to the values they take at TRs in the range $1.2 \le TR \le 2.0$, whilst keeping all other local surface BCs (η_{ML}, $\bar{k}_w$, h_c and λ) equal to the values they take in a converged simulation at the reference TR. If linear superposition can be assumed to be valid, this allows us to determine the impact on θ of changes in h_m (with TR) for fixed conditions of other local surface BCs. We refer to these changes as $\Delta\theta_{E3}(x)$, where the sign convention is $\Delta\theta_{E3}(x) = \theta(x) - \theta(x)^{TR=2.0}$. The changes $\Delta\theta_{E3}(x)$ are plotted for the range $1.2 \le TR \le 2.0$ in Fig. 14.

The effect of reducing TR from the reference condition is to increase external heat transfer coefficient, which reduces θ due to higher external heat transfer. This effect occurs because of an increase in $Nu_m(x)$, which is caused by an increase in $Re_m(x)$. $Re_m(x)$ increases primarily because of an increase in $\rho_m(x)$ as we move from the reference TR to lower-than-reference TR. This is due to lower absolute mainstream temperature lowering the average absolute temperature of the mixing layer. There are smaller contributions of both positive and negative sign associated with changes in other variables. In order of decreasing absolute magnitude of effect these variables are: $k_m(x)$, $u_m(x)$, $\mu_m(x)$ and $c_{pm}(x)$. We discuss these smaller effects later in this section. The surface-mean changes in overall cooling effectiveness from the value for the reference TR, $\overline{\Delta\theta}_{E3}$, were −0.003, −0.007, −0.011, and −0.016 for TRs 1.8, 1.6, 1.4 and 1.2 respectively. As percentages of the target mean effectiveness ($\bar{\theta} = 0.500$) these are equivalent to changes of −0.60%, −1.40%, −2.20% and −3.20% respectively.

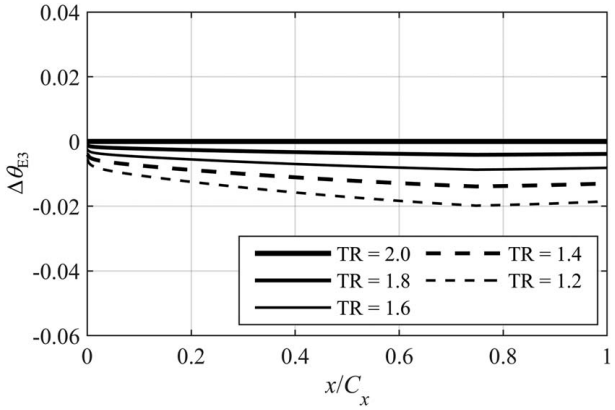

Fig. 14 Change in overall cooling effectiveness when external heat transfer coefficient, h_m, is changed—in isolation of other local surface BCs—from its value at reference TR

So far as the trends with surface distance are concerned, we see (Fig. 14) that the change, $\Delta\theta_{E3}(x)$, is greater at the trailing edge ($x/C_x = 1.0$) than the leading edge ($x/C_x = 0$) by a factor of approximately 3.2. To explain why the magnitude of change increases with surface distance we consider the sensitivity of $\theta(x)$ to $h_m(x)$, i.e. the partial derivative of Eq. (11) with respect to $h_m(x)$

$$\frac{\partial\theta}{\partial h_m}(x) = \frac{-(\lambda(x) - \eta_{ML}(x))\left(\frac{1}{h_c(x)} + \frac{t_w}{\bar{k}_w(x)}\right)}{\left(1 + h_m(x)\left(\frac{1}{h_c(x)} + \frac{t_w}{\bar{k}_w(x)}\right)\right)^2} \tag{30}$$

The partial derivative of Eq. (11) with respect to $h_m(x)$ is plotted in Fig. 15 as a function of x/C_x. We also plot the change in $h_m(x)$, $\Delta h_m(x)$, between the reference TR (TR = 2.0) and the case of TR = 1.2 (arbitrary choice). We normalise by values at the leading edge of the plate ($x/C_x = 0$) for which numerical values are: $\partial\theta/\partial h_m = -4.7 \times 10^{-5}\,\mathrm{W^{-1}\,m^2K}$ and $\Delta h_m = -128\,\mathrm{W\,m^{-2}K^{-1}}$. We see that the general trend with x for the magnitude of $\partial\theta/\partial h_m$ is to increase from the leading edge to plane 2 ($x/C_x = 0.75$) and decrease from plane 2 to the trailing edge. This trend is driven primarily by the term $\lambda(x) - \eta_{ML}(x)$ (Eq. (30)), which increases with surface distance in the region of the leading circuit (dominated by reduction in $\eta_{ML}(x)$) and decreases with surface distance in the region of the trailing circuit (dominated by reduction in $\lambda(x)$). Looking at the change in $h_m(x)$ between TR = 2.0 and TR = 1.2 (arbitrary choice) we see that the magnitude of $\Delta h_m(x)$ is approximately constant over most of the surface (apart from a significant reduction at the leading edge). Taken in combination the trends for $\partial\theta/\partial h_m$ and $\Delta h_m(x)$ lead to an increasing trend with surface distance in the absolute value of term $\Delta\theta_{E3}(x)$ between planes 1 and 2 and a decreasing trend between planes 2 and 3.

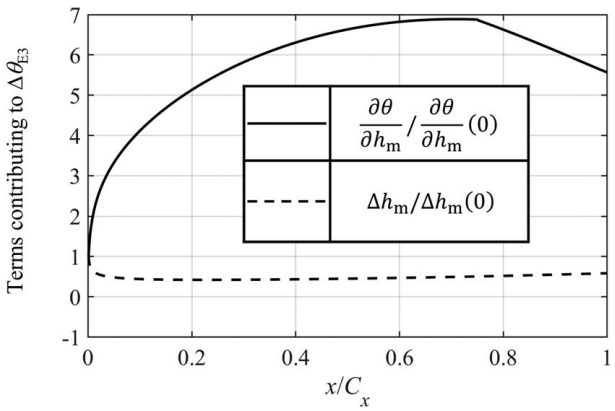

Fig. 15 Terms contributing to changes in θ caused by changes in h_m, in isolation of other local surface BCs. Both terms are normalised by their respective values at $x/C_x = 0$.

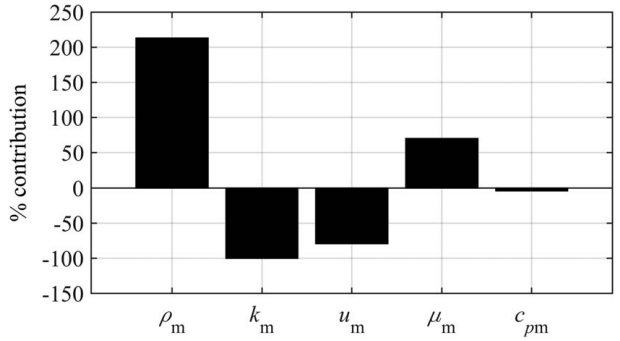

Fig. 16 Percentage contributions of five underlying terms to changes in surface-averaged external heat transfer coefficient, $\bar{h}_m$

Recall that $h_m(x)$ increases as we move from the reference TR to lower-than-reference TR because of an increase in $Nu_m(x)$, due to an increase in $Re_m(x)$, which is a consequence of an increase in $\rho_m(x)$. To provide insight into second-order effects, we now perform a sensitivity analysis of all influences on $h_m(x)$ as TR is varied. Substituting Eq. (21) into Eq. (22) external heat transfer coefficient can be expressed as

$$h_m(x) = 0.0296x^{-1/5}\rho_m(x)^{4/5}u_m(x)^{4/5}\mu_m(x)^{-7/15}k_m(x)^{2/3}c_{pm}(x)^{1/3} \tag{31}$$

We evaluate the approximate percentage contribution of each variable to changes in surface-averaged external heat transfer coefficient, $\bar{h}_m$, by considering the partial derivative of Eq. (31) with respect to each of $\rho_m(x)$, $k_m(x)$, $u_m(x)$, $\mu_m(x)$ and $c_{pm}(x)$. The results are presented as a bar chart in Fig. 16.

Positive percentage contribution implies that the change in that variable—in isolation of all other variables—as we move from the reference TR to lower-than-reference TR causes an increase in $\bar{h}_m$. Looking at the figure, we see that the increase in $\bar{h}_m$ with reducing TR is dominated by the increase in $\rho_m(x)$. This effect has been discussed. There is an additional contribution of the same sign caused by a decrease in $\mu_m(x)$ ($\sqrt{T_m}$ dependence; note negative exponent for μ_m in Eq. (31)) with TR, caused by a reduction in static temperature of the mixing layer, T_m, which is driven by a reduction in mainstream total temperature, T_{01h}. There are terms of opposite sign associated with decreases in k_m and u_m ($\sqrt{T_m}$ dependence; note positive exponents in Eq. (31)). The contribution associated with the change in c_{pm} is small in comparison to other terms.

In summary, as we move from the reference TR to lower-than-reference TR, there is an increase in external heat transfer coefficient, $h_m(x)$, which causes a decrease in θ. This effect occurs because of an increase in $Nu_m(x)$, which is caused by an increase in $Re_m(x)$. $Re_m(x)$ increases primarily because of an increase in $\rho_m(x)$ as we move from the reference TR to lower-than-reference TR. This is due to lower absolute mainstream temperature lowering the average absolute temperature of the mixing layer. There are four additional effects, but they are substantially smaller in magnitude and partially cancel each other out.

Effect 4: Changes in Overall Cooling Effectiveness due to Changes in Internal Heat Transfer Coefficient. We now consider the effect on θ of varying internal heat transfer coefficient (h_c)—in isolation of other local surface BCs—from its value at the reference TR. We change the distributions $h_c(x)$ to the values they take at TRs in the range $1.2 \le TR \le 2.0$, whilst keeping all

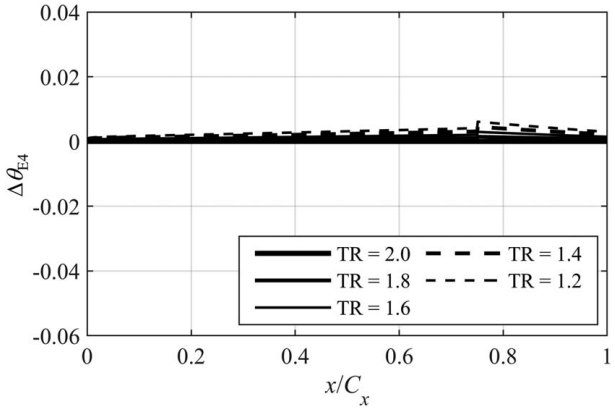

Fig. 17 Change in overall cooling effectiveness when internal heat transfer coefficient, h_c, is changed—in isolation of other local surface BCs—from its value at reference TR

other local surface BCs (η_{ML}, $\bar{k}_w$, h_m and λ) equal to the values they take in a converged simulation at the reference TR. If linear superposition can be assumed to be valid, this allows us to determine the impact on θ of changes in h_c (with TR) for fixed conditions of other local surface BCs. We refer to these changes as $\Delta\theta_{E4}(x)$, where the sign convention is $\Delta\theta_{E4}(x) = \theta(x) - \theta(x)^{TR=2.0}$. The changes $\Delta\theta_{E4}(x)$ are plotted for the range $1.2 \le TR \le 2.0$ in Fig. 17.

The surface-mean changes in overall cooling effectiveness from the value for the reference TR, $\overline{\Delta\theta}_{E4}$, were 0.0008, 0.0016, 0.0023, and 0.0031 for TRs 1.8, 1.6, 1.4 and 1.2 respectively. As percentages of the target mean effectiveness ($\theta = 0.500$) these are equivalent to changes of 0.16%, 0.32%, 0.46% and 0.62% respectively. That is, the impact is a small increase in overall cooling effectiveness.

The effect of reducing TR from the reference condition is to very slightly increase the internal heat transfer coefficient, which slightly increases θ due to higher internal heat transfer. We now explain this effect in detail. Substituting Eq. (14) into Eq. (15), internal heat transfer coefficient can be expressed as

$$h_c(x) = 0.023 D(x)^{-0.2} (\rho_c(x) u_c(x))^{0.8} c_{pc}(x)^{0.4} \mu_c(x)^{-0.4} k_c(x)^{0.6} \quad (32)$$

The reason for an increase in $h_c(x)$ as we reduce TR is an increase in the product of local coolant density and velocity, $\rho_c(x)u_c(x)$, due to a (slight) increase in duct-averaged density, $\bar{\rho}_c$. This is equivalent to coolant mass flow rate increasing. The physical basis for the increase in mass flow rate, is that, as TR is reduced, ρ_c has lower heat pick-up with local surface distance (from cooling channel inlet), leading to lower decrease in ρ_c with surface distance. This effect arises because at lower TR the mainstream flow has lower absolute driving temperature.

Duct-averaged velocity, $\bar{u}_c$, is approximately invariant with TR and therefore its contribution to changes in mass flow rate is second order. As we move from the reference TR to lower-than-reference TR we observe the following interrelated effects: a very small reduction in static pressure at the leading edge, p_1; and a very small increase in dynamic head at the film cooling hole *exit*, $\rho'_{1c}u'^2_{1c}$; a very small increase in channel total pressure loss, $p_{02c} - p_{01c}$; an increase in $\bar{\rho}_c$ due to lower mean T_c; a reduction in $\bar{u}_c$ due to lower mean T_c; negligible change in $\bar{u}_c$. Cause and effect is rather moot because all changes are arguably inter-related.

Here we have explained trends in term of duct-average values. Whilst the arguments are true, consider also that at the cooling duct inlet ($x/C_x = 0.75$) $\Delta\theta_{E4}(x)$ takes its maximum value, but, apparently contradictorily, here the change in h_c must be attributed only to changes in u_c, the other variables (ρ_c, k_c, μ_c, and c_{pc}) being fixed by the cooling system inlet BCs at this position, and therefore not varying with TR. The mystery is explained considering mass conservation more deeply.

It is worth noting that whilst for the fixed-PR domain-global BC the impact on θ of changes in h_c with TR is small, this is not the case for the domain-global BC of fixed exit-Re *and* fixed PR. It is for this reason that we discuss the effects in full, because the *mechanisms* for sensitivities are similar for both types of domain-global BC. We consider the effect of changing domain-global BCs in a later section.

So far as the trends with surface distance are concerned, we see (Fig. 17) that the change $\Delta\theta_{E4}(x)$ is greater at location of the cooling channel inlets ($x/C_x = 0.75$) than at the leading and trailing edges ($x/C_x = 0$ and $x/C_x = 1$ respectively). This is explained by the following logic. There is a global increase in $h_c(x)$ with decreasing TR arising from increased $\rho_c(x)$, which causes a global increase in θ. The product $\rho_c(x)u_c(x)$ is constant along the duct (conservation of mass) so this term in Eq. (32) can be thought of as being responsible for the offset but not the secondary trend. In general (for all TR conditions) there is heat pick up in the coolant flow, increasing in the streamwise direction away from the coolant inlet ($x/C_x = 0.75$). This causes an increase in $k_c(x)$ with streamwise distance ($\sqrt{T_c}$ dependence). The increase in $k_c(x)$ with streamwise distance increases $h_c(x)$ with streamwise distance (see Eq. (32)) which increases θ with streamwise distance. Because the effect is related to the square root of *absolute* temperature it is larger for TR = 2.0 than for lower temperature ratio conditions. When differences $\Delta\theta_{E4}(x)$ are taken, this leads to a negative trend of $\Delta\theta_{E4}(x)$ from the cooling channel inlets ($x/C_x = 0.75$), i.e. a maximum at ($x/C_x = 0.75$) and minima at ($x/C_x = 0$ and $x/C_x = 1$ respectively). Because the heat pick up is relatively small (values of $\lambda(x)$ close to unity) the trends are approximately linear (far from reaching asymptotic condition).

To provide insight into second-order effects, we now perform a sensitivity analysis of all influences on $h_c(x)$ as TR is varied. By considering the partial derivatives of Eq. (32) with respect to each of $\rho_c(x)$, $k_c(x)$, $u_c(x)$, $\mu_c(x)$ and $c_{pc}(x)$ we evaluate the approximate percentage contribution of each variable to changes in duct-averaged internal heat transfer coefficient, $\bar{h}_c$. The results are presented as a bar chart in Fig. 18. Positive percentage contribution implies that the change in that variable—in isolation of all other variables—as we move from the reference TR to lower-than-reference TR causes an increase in $\bar{h}_c$.

Looking at Fig. 18, we see that the increase in $\bar{h}_c$ with reducing TR is dominated by the increase in ρ_c. This effect has been discussed. There is an additional contribution of the same sign caused by a decrease in μ_c with TR ($\sqrt{T_c}$ dependence; note negative exponent for μ_c in Eq. (32)), caused by a reduction in surface-averaged static temperature of the coolant, $\bar{T}_c$, due to a reduction in *absolute* internal convective heat transfer rate as we reduce TR. There is a term of opposite sign associated with a decrease in k_c ($\sqrt{T_c}$ dependence; note positive exponent in Eq. (32)). The contributions associated with the changes in c_{pc}

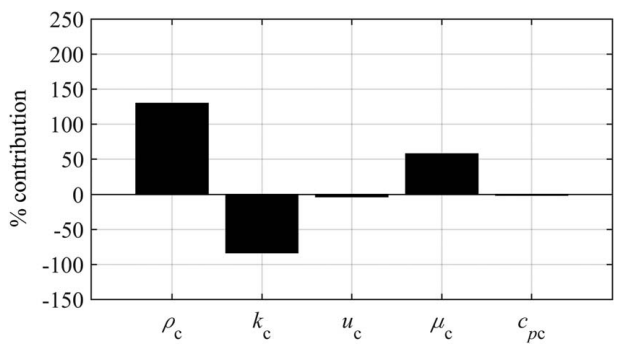

Fig. 18 Percentage contributions of five underlying terms to changes in surface-average internal heat transfer coefficient, $\bar{h}_c$

and u_c are small in comparison to other terms. We note that whilst the contribution of u_c to changes in *duct-averaged* internal heat transfer coefficient, $\bar{h}_c$, is small, the local effect can be significant. This apparent contradiction has been discussed.

In summary, as we move from the reference TR to lower-than-reference TR, there is an increase in internal heat transfer coefficient, $h_c(x)$, which causes an increase in θ. This is primarily driven by an increase in coolant density, $\rho_c(x)$, as we reduce TR. This is because of lower *absolute* heat transfer rate from internal wall to coolant, resulting in lower average absolute coolant temperature. There are four additional effects, but they are smaller in magnitude and partially cancel each other out.

Effect 5: Changes in Overall Cooling Effectiveness due to Changes in Internal Cooling Effectiveness. We now consider the effect on θ of varying internal cooling effectiveness (λ)—in isolation of other local surface BCs—from its value at the reference TR. We change the distributions $\lambda(x)$ to the values they take at TRs in the range $1.2 \le \mathrm{TR} \le 2.0$, whilst keeping all other local surface BCs (η_{ML}, $\bar{k}_w$, h_m and h_c) equal to the values they take in a converged simulation at the reference TR. If linear superposition can be assumed to be valid, this allows us to determine the impact on θ of changes in λ (with TR) for fixed conditions of other local surface BCs. We refer to these changes as $\Delta\theta_{E5}(x)$, where the sign convention is $\Delta\theta_{E5}(x) = \theta(x) - \theta(x)^{\mathrm{TR}=2.0}$. The changes $\Delta\theta_{E5}(x)$ are plotted for the range $1.2 \le \mathrm{TR} \le 2.0$ in Fig. 19.

The effect of reducing TR from the reference condition is to reduce internal cooling effectiveness (greater *non-dimensional* temperature rise in the internal cooling flow), which decreases θ. This effect occurs because of a decrease in TR itself, an effect that arises in the system due to the combination of recovery ratios (i.e. this is a manifestation of the effect of compressibility on our chosen definition of λ). There are smaller contributions of both positive and negative sign associated with changes in other variables.

The surface-mean changes in overall cooling effectiveness from the value for the reference TR, $\overline{\Delta\theta}_{E5}$, were −0.0006, −0.0015, −0.0033, and −0.0081 for TR = 1.8, 1.6, 1.4 and 1.2 respectively. As percentages of the target mean effectiveness ($\overline{\theta} = 0.500$) these are equivalent to changes of −0.12%, −0.30%, −0.66% and −1.62% respectively.

So far as the trends with surface distance are concerned, we see (Fig. 19) that the change, $\Delta\theta_{E5}(x)$, increases in magnitude with surface distance. For the TR = 1.2 case (arbitrary choice), the magnitude of correction is larger at the trailing edge than the leading edge by factor 10.6. To explain why the magnitude of correction increases with surface distance, we consider the partial derivative of θ with respect to λ i.e. the partial derivative of Eq. (11) with respect to λ

$$\frac{\partial\theta}{\partial\lambda}(x) = \frac{1}{1 + h_m(x)\left(\frac{1}{h_c(x)} + \frac{t_w}{\bar{k}_w(x)}\right)} \tag{33}$$

This is plotted in Fig. 20 as a function of x/C_x. We also plot the change in $\lambda(x)$, $\Delta\lambda(x)$, between the reference TR (TR = 2.0) and the case of TR = 1.2 (arbitrary choice). Both terms are normalised by their respective values at $x/C_x = 0$, which are 0.19 and −0.012 for $\partial\theta/\partial\lambda$ and $\Delta\lambda(x)$, respectively.

We see that the general trend with x for the magnitude of $\partial\theta/\partial\lambda$ is to increase from the leading edge to a maximum at $x/C_x = 0.44$ and decrease (slightly) from $x/C_x = 0.44$ to the trailing edge. This is primarily driven by the distribution of $h_m(x)$ (see discussion in the context of Fig. 6), whilst there are second order contributions from the distributions of $h_c(x)$ and $\bar{k}_w(x)$.The general trend for the magnitude of $\Delta\lambda(x)$ is quasi-exponential increase from the leading edge to trailing edge. Taken in combination, the trends for $\partial\theta/\partial\lambda$ and $\Delta\lambda(x)$ lead to an increasing trend with surface distance in the absolute value of $\Delta\theta_{E5}(x)$ between the leading edge and trailing edge. As we will see in a moment, changes in λ are dominated by changes in TR (definitional issue) and, by considering the partial derivative of λ with respect to TR, $\partial\lambda(x)/\partial\mathrm{TR}$ (not shown), we see that the shape of the trend for $\Delta\lambda(x)$ with surface distance is dominated by a combination of the distributions $c_c(x)$ and $c_h(x)$. TR and the change in TR, ΔTR, are—by definition—constant with surface distance. The effect of compressibility in the system (i.e. recovery ratios less than unity) is to reduce λ (compared to the case $c_c(x) = c_h(x) = c_m(x) = 1$). For temperature ratios greater than unity, the effect of decreasing TR from TR = 2.0 is to amplify the magnitude of the reduction in λ caused by this compressibility effect.

Recall that $\lambda(x)$ decreases as we move from the reference TR to lower-than-reference TR, and does so definitionally because of a reduction in TR itself. This definitional change is the primary effect. To provide insight into second-order effects, we now perform a sensitivity analysis of all influences on $\lambda(x)$ as TR is varied. The full equation for internal cooling effectiveness arises from energy conservation within the internal cooling duct. Taking the approximation of constant specific heat capacity of the coolant within the leading circuit (i.e. $c_{pc}(x) = c_{p2c}$) and using a local co-ordinate system based on streamwise distance from the channel inlet, x' (where $x' = 0.75C_x - x$ for the leading circuit, and $x' = x - 0.75C_x$ for the TE circuit), applying an energy balance for the internal coolant stream gives the following

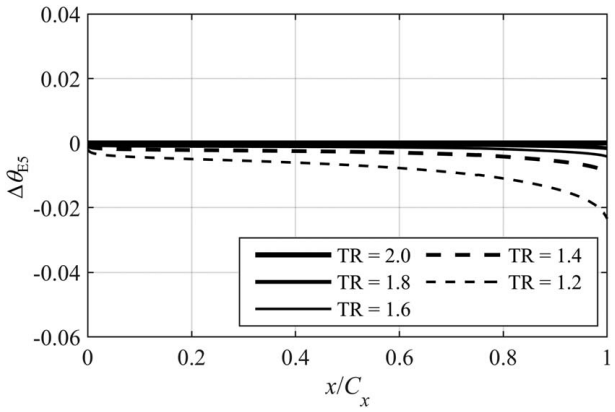

Fig. 19 Change in overall cooling effectiveness when internal cooling effectiveness, λ, is changed—in isolation of other local surface BCs—from its value at reference TR

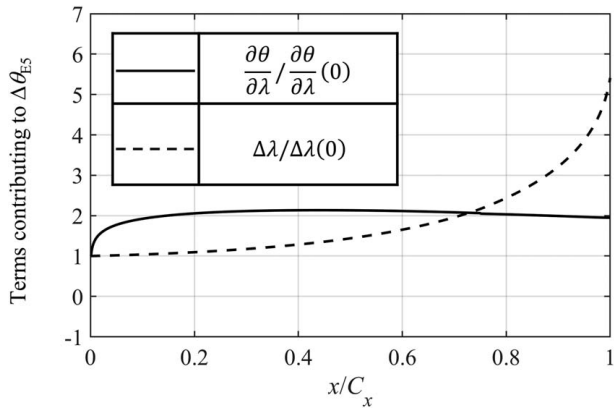

Fig. 20 Terms contributing to changes in θ caused by changes in λ, in isolation of other local surface BCs. Both terms are normalised by their respective values at $x/C_x = 0$.

distribution $\lambda(x')$

$$\lambda(x') = \lambda(0) - \int_0^{x'} \left(\frac{(1-\lambda(x'))\mathrm{TR}}{(c_c(x') - c_h(x')\mathrm{TR})} \frac{\mathrm{d}c_h(x')}{\mathrm{d}x'} \right) \mathrm{d}x' - \int_0^{x'} \left(\frac{\lambda(x')}{(c_c(x') - c_h(x')\mathrm{TR})} \frac{\mathrm{d}c_c(x')}{\mathrm{d}x'} \right) \mathrm{d}x' - \int_0^{x'} \left(\frac{h_c(x')w}{\dot{m}_{1c}c_{p2c}} \right) (\lambda(x') - \varphi(x')) \mathrm{d}x' \quad (34)$$

where we define an *internal surface effectiveness*, $\varphi(x)$ by

$$\varphi(x) = \frac{c_h(x)T_{01h} - T_{w2}(x)}{c_h(x)T_{01h} - c_c(x)T_{02c}} \quad (35)$$

where $T_{w2}(x)$ is wall internal surface temperature and where we note the analogy to the definition of $\theta(x)$ (see Eq. (2)). We make the further assumption that the recovery ratios are invariant of TR, so that—so far as variation with TR is concerned—the functional form of Eq. (34) is $\lambda = f(\mathrm{TR}, \varphi, h_c, \dot{m}_{1c}c_{p2c})$: i.e. a function of four groups. We evaluate the sensitivity of surface-averaged internal cooling effectiveness, $\bar{\lambda}$, to each of the four groups by partial derivatives of Eq. (34) with respect to each group in turn. Percentage contributions of each variable to the overall change in surface-averaged internal cooling effectiveness ($\Delta\bar{\lambda}$) are presented as a bar chart in Fig. 21. Positive percentage contribution implies that the change in that variable—in isolation of all other variables—as we move from the reference TR to lower-than-reference TR causes a reduction in $\bar{\lambda}$ (greater rate of warming). Looking at the figure, we see that the reduction in $\bar{\lambda}$ as we reduce TR is dominated by reduction in TR itself. This effect arises due to the definitions of λ and θ, in combination with distributions of recovery ratios $c_c(x)$ and $c_h(x)$. Though purely definitional in nature, the term is real so far as scaling between temperature ratios is concerned.

A smaller effect with positive contribution arises because of a decrease in φ. We now explain this effect in detail. Moving from the reference TR to $\mathrm{TR} = 1.2$, the surface-averaged overall cooling effectiveness, $\bar{\theta}$, changes by −8.0% (see discussion in context of Fig. 8), and the surface-averaged internal surface effectiveness, $\bar{\varphi}$ changes by −7.0%. That is, both the inner and outer walls move in the direction of being non-dimensionally warmer. The non-dimensionally warmer internal wall leads to a faster rate of non-dimensional warming of coolant with local surface distance along the duct, or a faster rate of decrease of $\lambda(x)$ (see Eq. (7)). The effect of λ decreasing (coolant becoming non-dimensionally warmer)—in isolation of other local surface BCs—is to reduce non-dimensional internal convective heat transfer rate, which has the effect of reducing θ (wall moving towards being non-dimensionally warmer).

A smaller effect also with positive contribution arises because of an increase in internal heat transfer coefficient, $h_c(x)$, as we decrease TR. This is primarily due to an increase in the product of local coolant density and velocity, $\rho_c(x)u_c(x)$, due to an increase in surface-averaged coolant density, $\bar{\rho}_c$, as we move from the reference TR to lower-than-reference TR. This has been discussed in detail in the context of Fig. 17. An increase in $h_c(x)$ leads to an increase in internal convective heat transfer rate (wall to coolant), which leads to a higher rate (with x) of temperature rise in the internal cooling flow and lower internal cooling effectiveness.

Another small effect of negative sign arises because of an increase in local coolant heat capacity flow rate, $\dot{m}_{1c}c_{p2c}$, as we decrease TR. This is primarily due to an increase in coolant mass flow rate, caused by a higher average coolant density. Higher coolant capacity flow rate leads to a lower temperature rise in the internal cooling flow and a higher surface-average internal cooling effectiveness.

The effects of decreasing TR and increasing φ and h_c account for +88.1%, +13.5% and +3.7% of the overall change in λ, respectively, and are offset by a −5.3% contribution associated with changes in $\dot{m}_{1c}c_{p2c}$.

In summary, as we move from the reference TR to lower-than-reference TR, the internal cooling effectiveness, λ, decreases (coolant becomes non-dimensionally warmer), which leads to a reduction in θ. This effect is primarily definitional, and arises directly as a result of changes in TR, in combination with the definitions of λ and θ and distributions of recovery ratios $c_c(x)$ and $c_h(x)$. Though definitional in origin, it is real so far as scaling is concerned between different TR conditions. Three secondary effects arise due to changes in λ arising from internal surface effectiveness, $\varphi(x)$, internal heat transfer coefficient, $h_c(x)$, and local coolant heat capacity flow rate, $\dot{m}_{1c}c_{p2c}$. These are small in comparison to the primary term.

Comparison of Checksum of Changes in Overall Cooling Effectiveness due to Each Local Surface Boundary Condition With Overall Change. In this section we compare the overall change in θ, $\Delta\theta^{\mathrm{TR}=1.2}$, as we move from the reference TR to lower than reference TR with the checksum of changes in θ for each of effect 1 to effect 5 (i.e. $\sum_{j=1}^{5} \Delta\theta_{\mathrm{E}j}$). We do this (arbitrarily) for $\mathrm{TR} = 1.2$, for system 1 and the domain-global BC of fixed PR. The results we report are equally valid for other choices. The comparison is shown in Fig. 22. Looking at the figure, we see that the trends for the overall change and checksum are very similar (mean values of −0.041 and −0.041, respectively, with RMS difference between the trends of 0.0004 and maximum difference 0.0009). This demonstrates that linear superposition of the decomposed contributions (due to each of each of the five local surface BCs $\eta_{\mathrm{ML}}(x)$, $\bar{k}_w(x)$, $h_m(x)$, $h_c(x)$ and $\lambda(x)$) is valid to a high degree of accuracy. This justifies the assumptions made regarding

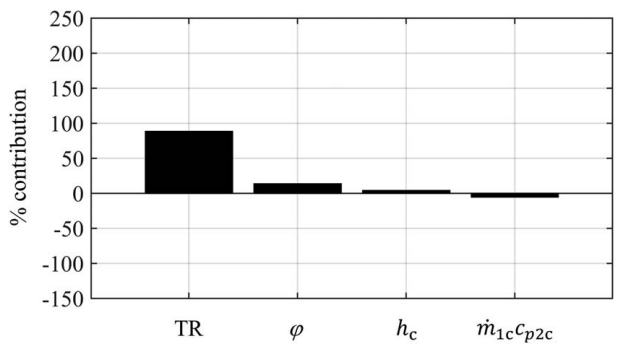

Fig. 21 Percentage contributions of four underlying terms to changes in surface-averaged internal cooling effectiveness, $\bar{\lambda}$

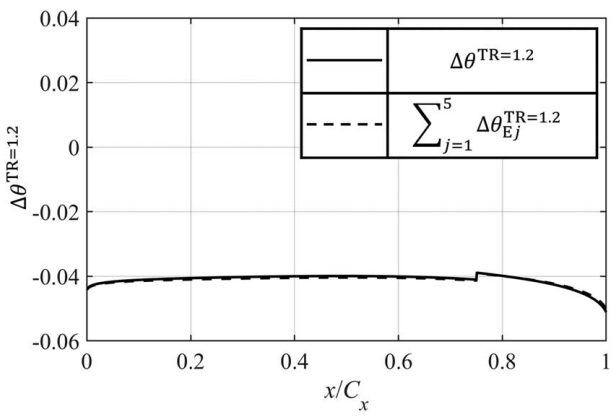

Fig. 22 Comparison of overall change in cooling effectiveness with checksum of contributions from each of effect 1 to effect 5. Result is between the reference TR and TR = 1.2

the use of a one-dimensional model to do simplified decomposition of the result.

Results IV: Sensitivity of Results to Domain-Global Boundary Conditions

In this section we compare the change in overall cooling effectiveness with TR for two domain-global boundary conditions common in experimental work: fixed PR (we will refer to BC1); and fixed exit-Re with fixed PR (we will refer to BC2). We show that the change in θ with TR is similar for these two typical boundary conditions.

We present in Fig. 23 the change in θ from the reference TR to TR = 1.2 ($\Delta\theta^{\mathrm{TR}=1.2} = \theta^{\mathrm{TR}=1.2} - \theta^{\mathrm{TR}=2.0}$) as a function of surface distance for both domain-global BCs. Results are (arbitrarily) for system 1. The distributions, $\Delta\theta^{\mathrm{TR}=1.2}(x)$, are similar for the two domain-global BCs, with values being bounded by $-0.054 < \Delta\theta^{\mathrm{TR}=1.2}(x) < -0.036$, and with mean values $\overline{\Delta\theta}^{\mathrm{TR}=1.2} = -0.041$ and -0.043, for BC1 and BC2 respectively. The RMS difference between trends was 0.003, and maximum absolute difference was 0.006. The trend for BC1 was discussed in the context of Fig. 8. Although the trend for BC2 is similar, the physical bases for this is different. We will discuss this in detail.

We now quantify and compare the percentage contributions of each of effects 1–5 to changes with TR in surface averaged $\theta(x)$, $\Delta\bar{\theta}^{\mathrm{TR}=1.2}$, for BC1 and BC2. Results are presented in Fig. 24. Looking at the figure, we see that the percentage contributions of $\eta_{\mathrm{ML}}(x)$, $\bar{k}_{\mathrm{w}}(x)$ and $\lambda(x)$ to changes in $\bar{\theta}$ are very similar for BC1 and BC2, whereas the percentage contributions arising from $h_{\mathrm{m}}(x)$ and $h_{\mathrm{c}}(x)$ are very different for the two domain-global BCs. This

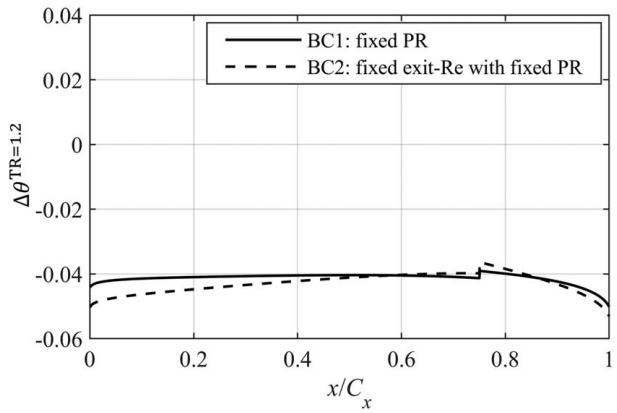

Fig. 23 Changes in overall cooling effectiveness between the reference TR and TR = 1.2 as a function of surface distance for two domain-global boundary conditions

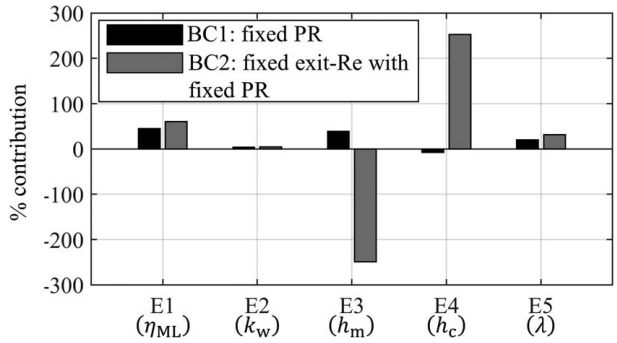

Fig. 24 Percentage contributions of each of effects 1–5 to changes in surface-averaged overall cooling effectiveness for two types of domain-global BC. Results are shown for system 1.

is in spite of the *overall* change (Fig. 23) being similar. As we move from BC1 to BC2 the contributions from $h_{\mathrm{m}}(x)$ and $h_{\mathrm{c}}(x)$ become much larger in absolute magnitude, but have opposite sign and almost cancel each other out.

First, consider the effect of changes in $\eta_{\mathrm{ML}}(x)$ on changes in $\bar{\theta}$ as we move from the reference TR to lower-than-reference TR. We saw (discussion in context of Figs. 11 and 12) that changes in $\eta_{\mathrm{ML}}(x)$ were dominated by changes in the ratio of integrated (between 0 and x) entrainment mass flow rate and coolant mass flow rate at plane 1 ($\dot{m}_{\mathrm{e}}(x)/\dot{m}_{1\mathrm{c}}$). This, in turn, was dominated by changes in density ratio $\rho_{1\mathrm{c}}/\rho_{1\mathrm{h}}$ with TR. This change is approximately independent of the choice of domain-global BC, explaining the similar results for BC1 and BC2 in Fig. 24.

Now we consider the effect of changes in $\bar{k}_{\mathrm{w}}(x)$ on changes in $\bar{\theta}$ as we move from the reference TR to lower-than-reference TR. The percentage contribution of $\bar{k}_{\mathrm{w}}(x)$ to changes in $\bar{\theta}$ is very similar for BC1 and BC2 (and much smaller in magnitude than the other effects) because changes in $\bar{k}_{\mathrm{w}}$ are caused by changes in T_{w}, which are similar for both BC1 and BC2.

Now we consider the effect of changes in $h_{\mathrm{m}}(x)$ and $h_{\mathrm{c}}(x)$ on changes in $\bar{\theta}$ as we move from the reference TR to lower-than-reference TR. As we move from BC1 to BC2, the percentage contributions of $h_{\mathrm{m}}(x)$ and $h_{\mathrm{c}}(x)$ to changes in $\bar{\theta}$ become significantly larger in magnitude and change in sign. Despite this significant change, it happens that the combined effects of $h_{\mathrm{m}}(x)$ and $h_{\mathrm{c}}(x)$ essentially cancel for both BC1 and BC2. Consider first that it is primarily the *ratio* $h_{\mathrm{m}}(x)/h_{\mathrm{c}}(x)$ that affects $\theta(x)$ (see Eq. (11)): the absolute values $h_{\mathrm{m}}(x)$ and $h_{\mathrm{c}}(x)$ are of secondary importance. If the ratio were insensitive to the domain-global BCs it would explain this effect. We can show that this is so by taking the ratio of Eqs. (5) and (6) and substituting in Eqs. (14) and (21), as well as the definitions of Reynolds number and mass flow rate. We arrive at

$$\frac{h_{\mathrm{m}}(x)}{h_{\mathrm{c}}(x)} = \left(\left(1 + \frac{\dot{m}_{\mathrm{e}}(x)}{\dot{m}_{1\mathrm{c}}}\right)\frac{\mu_{\mathrm{c}}(x)}{\mu_{\mathrm{m}}(x)}\frac{H(x)wx}{D(x)A_{\mathrm{m}}(x)}\right)^{0.8} \times \frac{\mathrm{Pr}_{\mathrm{m}}(x)^{\frac{1}{3}}}{\mathrm{Pr}_{\mathrm{c}}(x)^{0.4}}\frac{k_{\mathrm{m}}(x)}{k_{\mathrm{c}}(x)}\frac{D(x)}{x} \tag{36}$$

In Eq. (36) $h_{\mathrm{m}}/h_{\mathrm{c}}$ as expressed a function of six groups i.e. $h_{\mathrm{m}}/h_{\mathrm{c}} = f(\dot{m}_{\mathrm{e}}/\dot{m}_{1\mathrm{c}}, k_{\mathrm{c}}/k_{\mathrm{m}}, \mu_{\mathrm{c}}/\mu_{\mathrm{m}}, \mathrm{Pr}_{\mathrm{m}}, \mathrm{Pr}_{\mathrm{c}}, Hwx/DA_{\mathrm{m}})$. We consider how the variation of each of these groups with TR is affected by the domain-global BCs. We have already established that the change in $\dot{m}_{\mathrm{e}}/\dot{m}_{1\mathrm{c}}$ with TR is approximately independent of the choice of domain-global BC. The fluid properties (k_{m}, μ_{m}) and Prandtl number (Pr_{m}) of the mixing layer are functions of the static temperature, $T_{\mathrm{m}}(x)$. This is determined by the external Mach number distribution (approximately invariant of TR) and the total temperature of the mixing layer, $T_{0\mathrm{m}}(x)$. $T_{0\mathrm{m}}(x)$ is determined by considering mass and energy conservation and can be shown (substitution of Eq. (29) into Eq. (26)) to be a function of six groups, $T_{0\mathrm{m}} = f(\dot{m}_{\mathrm{e}}(x)/\dot{m}_{1\mathrm{c}}, c_{p01\mathrm{h}}/c_{p1\mathrm{c}}, T_{01\mathrm{h}}, T_{02\mathrm{c}}, \dot{m}_{1\mathrm{c}}/\dot{m}_{3\mathrm{c}}, \varepsilon)$. The variation of $c_{p01\mathrm{h}}/c_{p1\mathrm{c}}$ with TR is approximately independent of the choice of domain-global BC. The cooling system BCs $T_{01\mathrm{h}}$ and $T_{02\mathrm{c}}$ are fixed, and are therefore inherently independent of the choice of domain-global BC. The groups $\dot{m}_{1\mathrm{c}}/\dot{m}_{3\mathrm{c}}$ and ε are approximately unchanged with TR. For these reasons $T_{0\mathrm{m}}$ is essentially unaltered with the change in domain-global BCs. Consequently, the effects of changes in k_{m}, μ_{m} and Pr_{m} on $h_{\mathrm{m}}/h_{\mathrm{c}}$ are approximately independent of the choice of domain-global BC. So far as Pr_{c} is concerned, the variation with TR of internal coolant fluid properties k_{c}, μ_{c} and c_{pc} are relatively small (see discussion in the context of Fig. 18) and similar for both domain-global BCs (driven by θ which is similar for both BCs) and therefore the change in Pr_{c} with TR is relatively small, and the change between BC1 and BC2 at a given TR even smaller. Finally, the group Hwx/DA_{m} is determined by geometry and does not depend on the domain global BCs. In practice then, all six of the groups on which $h_{\mathrm{m}}/h_{\mathrm{c}}$ is functionally dependent have a variation with TR that is similar for BC1 and BC2. This means that $h_{\mathrm{m}}/h_{\mathrm{c}}$ has similar variation with TR for both domain-global BCs. For this reason, even though there is a significant decrease in the magnitude of both h_{m}

and h_c for low-TR conditions for BC2 (the decrease in h_m is caused by a decrease in k_m with TR, where we note that Re_m and therefore Nu_m are approximately invariant of TR due to the constraint of fixed exit Re; the decrease in h_c is caused by a reduction in Re_c due to a decrease in ρ_c as we reduce p_{02c} with TR in order to maintain a fixed CMPR), because the ratio h_m/h_c is approximately preserved with TR there is little impact on $\bar{\theta}$.

Finally, we consider the effect of changes in $\lambda(x)$ on changes in $\bar{\theta}$ as we move from the reference TR to lower-than-reference TR. We saw in Results III that changes in $\lambda(x)$ were dominated by changes in TR. We described this as a definitional issue. This definitional issue is independent of the choice of domain-global BC, explaining the similar results for BC1 and BC2 in Fig. 24.

In summary changes in $\theta(x)$ with TR are similar for both types of domain-global BCs typical in experimental work. This is because θ is functionally dependent on η_{ML}, $\bar{k}_w$, h_m/h_c, and λ, and the changes of these groups with TR are similar for the two types of domain-global BC.

Results V: Sensitivity of Results to Mean Value of Overall Cooling Effectiveness

In this section we consider the sensitivity of our results to the mean value of overall cooling effectiveness. Results are arbitrarily presented for system 1, but are equally applicable to other systems. We explore three values of mean overall cooling effectiveness at the reference TR, $\bar{\theta}^{TR=2.0} = 0.4, 0.5, 0.6$, which cover the typical range for HPNGVs (see, for example, Rhee et al. [21]). These mean values are achieved by introducing modified correlations for effectiveness of the mixing layer, $\eta'_{ML} = k_1\eta_{ML}$, local external Nusselt number, $Nu'_m = k_2 Nu_m$, and local cooling-channel Nusselt number, $Nu'_c = k_3 Nu_c$, where k_1, k_2 and k_3 are constants. We constrain these constants to the ranges $0.5 \le k_1 \le 2.5$ (so that η'_{ML} at the leading edge is constrained to the range $0.2 - 1.0$), $1 \le k_2 \le 2$ and $1 \le k_3 \le 2$ to ensure that we consider plausible deviations from the baseline correlations. There are infinite combinations of k_1, k_2 and k_3 that set a given value of $\bar{\theta}^{TR=2.0}$. For the $\bar{\theta}^{TR=2.0} = 0.4$ condition we do the following: vary k_1 alone; vary k_1 and k_2 together. For the $\bar{\theta}^{TR=2.0} = 0.6$ condition we do the following: vary k_1 alone; vary k_3 alone. By doing so we set extrema in the solution range (details beyond scope of discussion).

In Fig. 25 we present results for the surface-mean change in overall cooling effectiveness, $\overline{\Delta\theta}$, as a function of TR, for $\bar{\theta}^{TR=2.0} = 0.4$, 0.5 and 0.6. The range of TR was $1.1 \le TR \le 2.0$. Values of k_1, k_2 and k_3 are presented in the figure, and were chosen to represent solution-extrema. We see that all changes $\overline{\Delta\theta} = f(TR)$ are similar. The mean (across TR conditions) of the local RMS difference between lines (for all lines) normalized by the local value of $\Delta\theta$ was −0.072 (i.e. 7.2% of the local value).

The conclusion is that our general result is insensitive to the mean value of overall cooling effectiveness in the typical HPNGV range $0.4 < \bar{\theta}^{TR=2.0} < 0.6$. Interrogating the results (beyond the scope of this discussion) shows that physical arguments presented in the preceding sections remain valid at all mean values of overall cooling effectiveness considered.

In summary, the general results of this study are insensitive to the mean value of overall cooling effectiveness. This result is important because it demonstrates that the required correction offset for scaling overall cooling effectiveness from experimental to engine conditions is insensitive—over a fairly wide range—to non-dimensional operating temperature of the part.

Results VI: Sensitivity of Results to Internal Cooling System Network

In this section we compare results for internal cooling systems 1 to 3 (see Fig. 3), to understand the sensitivity of the results to the cooling system network. These three networks represent a fairly wide design range for HPNGV cooling systems

In Fig. 26, we present trends for $\Delta\theta^{TR=1.2}$ for all three cooling systems and the fixed-PR domain-global BC, BC1. Although we do not present results the same conclusions hold true for BC2. The trend for system 1 was discussed in the context of Fig. 8. The trends for systems 2 and 3 are extremely similar (mean values within 0.64% of each other; mean RMS difference between trends of 0.0004; maximum difference of 0.0017). The conclusion is that the general trend for the change in θ with TR is relatively independent of network choice.

In order to explain why the trends in $\Delta\theta^{TR=1.2}$ are very similar for each system, we compare the percentage contributions to $\Delta\theta^{TR=1.2}$ associated with each of five local surface BCs. These are presented in Fig. 27 for each of the three systems. Results are for BC1, but the general conclusions are equally applicable to BC2. Looking at the figure, we see that the percentage contribution of each local surface BC is almost identical between systems. We now discuss this result in detail.

The five effects driving changes in $\bar{\theta}$ with TR are changes in $\eta_{ML}(x)$, $\bar{k}_w(x)$, $h_m(x)$, $h_c(x)$ and $\lambda(x)$. We saw in Results III that the contribution of $\bar{k}_w(x)$ to changes in $\bar{\theta}$ with TR is second order and we saw in Results IV that $\bar{\theta}$ is insensitive to the absolute values of $h_m(x)$ and $h_c(x)$ as long as the ratio $h_m(x)/h_c(x)$ is preserved when TR is varied. Changes in $\bar{\theta}$ with TR are therefore driven by changes in $\eta_{ML}(x)$, $h_m(x)/h_c(x)$ and $\lambda(x)$ with TR. Changes in $\eta_{ML}(x)$ and $h_m(x)/h_c(x)$ with TR are caused primarily by changes in $\dot{m}_e(x)/\dot{m}_{1c}$ with TR (see Results IV), whilst changes in $\lambda(x)$ are

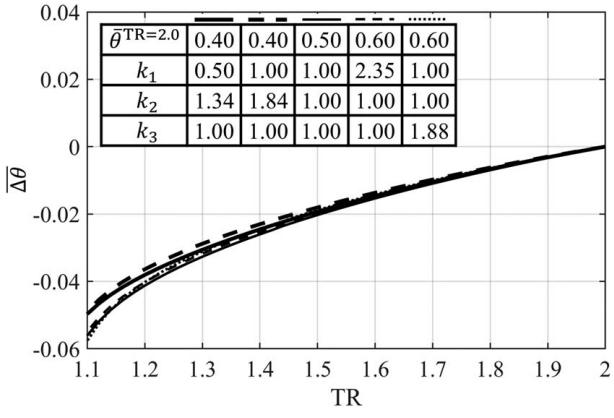

Fig. 25 Magnitude of surface-mean change in overall cooling effectiveness, $\overline{\Delta\theta}$, as a function of TR, for three values of mean overall cooling effectiveness, $\bar{\theta}^{TR=2.0}$, for different combinations of k_1, k_2, and k_3

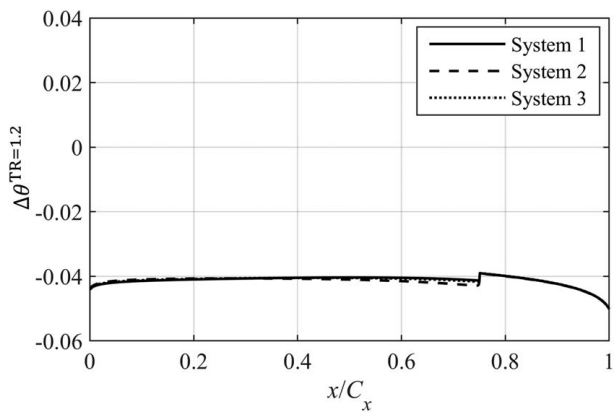

Fig. 26 Distributions of change in overall cooling effectiveness between the reference TR to TR = 1.2, $\Delta\theta^{TR=1.2}$, for cooling systems 1–3

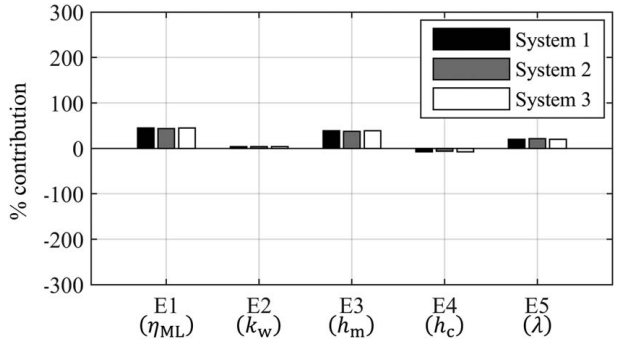

Fig. 27 Percentage contribution of each of five local surface BCs to changes in surface-averaged overall cooling effectiveness for systems 1 to 3 (domain-global BC of fixed PR)

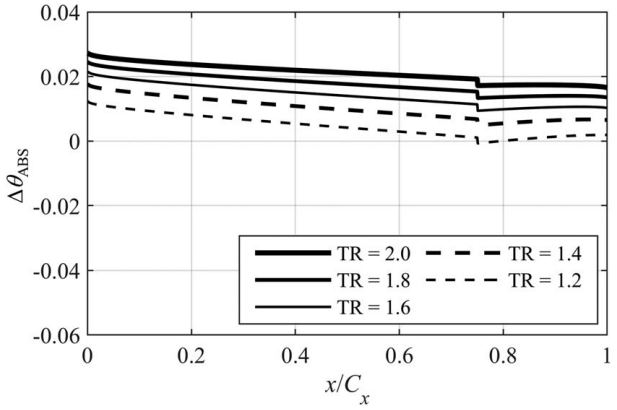

Fig. 28 Distributions of change in overall cooling effectiveness, $\Delta\theta_{ABS}(x)$, as we move from high absolute temperature to low absolute temperature as a function of normalised surface distance, x/C_x, for fixed temperature ratios in the range $1.2 \le TR \le 2.0$ (system 1 and domain-global boundary conditions of fixed PR)

dominated by changes in TR (definitional issue, see discussion in the context of Figs. 19 and 21). The differences in $\dot{m}_e(x)/\dot{m}_{1c}$ (for fixed TR) between systems originate from variation in channel pressure loss and internal convective heat transfer rate. These effects are small, so $\dot{m}_e(x)/\dot{m}_{1c}$ is approximately the same for all three cooling systems at a given TR. Thus, changes in $\eta_{ML}(x)$ and $h_m(x)/h_c(x)$ with TR are similar for all three cooling networks. TR itself is an input parameter, so inherently independent of cooling system choice. Thus, for a given TR, $\lambda(x)$ is approximately unchanged between cooling system network choices. The conclusion is that changes with TR in $\eta_{ML}(x)$, $h_m(x)/h_c(x)$ and $\lambda(x)$ and, therefore, $\bar{\theta}$ are approximately independent of the choice of cooling system.

In summary, we conclude that our general results are insensitive to the cooling system network over a fairly wide design range that includes most HPNGV cooling systems. We further show that changes due to each of the five local surface BCs are relatively similar in magnitude in all cases: that is, the driving effects are similar for this range of cooling systems.

Results VII: Sensitivity to Absolute Temperature

In this section we consider the sensitivity of our results to the absolute temperature. Typical engine mainstream and coolant total temperatures are 1750 K and 875 K [19]. To independently consider the impact of absolute temperature and TR we take the following: engine conditions as $T_{02c} = 875$ K and T_{01h} defined by TR; rig conditions as $T_{02c} = 300$ K with T_{01h} defined by TR. Fluid properties for air were taken from Poferl et al. [22] for high (engine) absolute temperatures and Oldfield and Guo [23] for low (rig) absolute temperatures. We refer to θ at engine (high) absolute temperatures as $\theta_{HT}(x)$, and θ at rig (low) absolute temperature as $\theta_{LT}(x)$. We refer to the change in overall cooling effectiveness as we move from the engine absolute temperatures to rig absolute temperatures as $\Delta\theta_{ABS}(x) = \theta_{LT}(x) - \theta_{HT}(x)$. We show that (at fixed TR) there is an increase in the magnitude of $\theta(x)$ as we move from high absolute temperature (typical engine values) to low absolute temperature (typical rig values). That is, cooling performance is overestimated at typical rig conditions.

The changes with absolute temperature in overall cooling effectiveness distribution at fixed TR for TRs in the range $1.2 \le TR \le 2.0$, $\Delta\theta_{ABS}(x)$, are shown in Fig. 28 for system 1 and the fixed-PR domain-global BC, BC1. The effect of moving from high absolute temperature to low absolute temperature *at fixed TR* is to increase effectiveness. This is caused by four effects. The first effect is an increase in $\theta(x)$ due to an increase in $h_c(x)$, which is caused by an increase in the product $\rho_c(x)u_c(x)$, due to an increase in $\bar{\rho}_c$ resulting from a decrease in $T_c(x)$ as we move from high absolute temperature to low absolute temperature. The second effect is a reduction in $\theta(x)$ due to an increase in $h_m(x)$, which is primarily driven by an increase in $\rho_m(x)$ and decrease in $\mu_m(x)$ as we move from high absolute temperature to low absolute temperature. The third effect is an increase in $\theta(x)$ due to an increase in $\eta_{ML}(x)$, which is caused by an increase in the ratio of coolant heat capacity flow rate to entrained hot-gas heat capacity flow rate ($\dot{m}_{1c}c_{p1c}/\dot{m}_e(x)c_{p01h}$), which is primarily due to an increase in the coolant-to-mainstream specific heat capacity (c_{p1c}/c_{p01h}) caused by a decrease in c_{p01h} as absolute temperature is reduced. The final effect is a reduction in $\theta(x)$ due to a decrease in $\bar{k}_w(x)$ due to a decrease in T_w as absolute temperature is reduced. There is an additional, second order contribution associated with an increase in $\lambda(x)$ as absolute temperature is reduced.

The surface-mean changes in overall cooling effectiveness as absolute temperature is reduced, $\overline{\Delta\theta}_{ABS}$, were +0.021, +0.018, +0.014, +0.010 and +0.005 for TRs 2.0, 1.8, 1.6, 1.4 and 1.2, respectively. As percentages of the mean effectiveness at high absolute temperature at each TR (0.479, 0.475, 0.470, 0.464 and 0.454 for TRs 2.0, 1.8, 1.6, 1.4 and 1.2, respectively) these are equivalent to changes of +4.38%, +3.71%, +3.02%, +2.16% and +1.02% respectively.

So far as the trends with surface distance are concerned, the positive values $\Delta\theta_{ABS}(x)$ (physical basis has been discussed) reduce with axial distance as we move from LE to the TE (factor of 1.8). This effect occurs primarily because the absolute increase in $\eta_{ML}(x)$ as absolute temperature is reduced is greater at the LE than the TE (see full discussion of this effect in the context of Figs. 8 and 11).

In summary, the effect of moving from high absolute temperature (engine) to low absolute temperature (rig) is an increase in $\theta(x)$, which is caused by the sum of effects of increases in $h_c(x)$, $h_m(x)$ and $\eta_{ML}(x)$ and a decrease in $\bar{k}_w(x)$. The implication is that overall cooling effectiveness is overestimated at lower absolute temperatures by typically 4.38% ($\bar{\theta} = 0.5$, TR = 2.0).

Results VIII: Effect of Combustion Product Gas Properties

In this section we consider the effect on our results of changing gas properties for the mainstream gas from those for combustion products (engine conditions) to air (typical lab conditions) at high absolute temperature. We do simulations over a range of TR, taking $T_{02c} = 875$ K and T_{01h} defined by TR. We show that—for fixed TR—there is an increase in the magnitude of $\theta(x)$ as we change gas properties from those for combustion products to those for air. We refer to θ evaluated using gas properties for combustion products as $\theta_{CP}(x)$, and θ evaluated using gas properties for air as $\theta_{Air}(x)$. We refer to the change in overall cooling effectiveness

as we change from gas properties (GP) for combustion products to those for air as $\Delta\theta_{GP}(x) = \theta_{Air}(x) - \theta_{CP}(x)$. Fluid properties for combustion products arising from burning kerosene in air (stoichiometric) were taken from Poferl et al. [22]. For the mixing layer we assume the fluid properties c_{pm}, k_m, R_m, γ_m and μ_m take the mass-averaged values of the mainstream (combustion products) and coolant (air) gasses at the local temperature of the mixing layer, T_m.

The changes in overall cooling effectiveness distribution at fixed TR for TRs in the range $1.2 \le TR \le 2.0$, $\Delta\theta_{GP}(x)$, are shown in Fig. 29 for system 1 and the fixed-PR domain-global BC, BC1. The effect of changing the mainstream gas from combustion products to air *at fixed TR* is to increase the overall cooling effectiveness. This is caused by two effects. The first effect is a decrease in $h_m(x)$, which is primarily driven by a decrease in $k_m(x)$. The second effect is an increase in $\eta_{ML}(x)$ due to an increase in the ratio of coolant heat capacity flow rate to entrained hot-gas heat capacity flow rate ($\dot{m}_{1c}c_{p1c}/\dot{m}_e(x)c_{p01h}$) caused by an increase in coolant-to-mainstream specific heat capacity ratio (c_{p1c}/c_{p01h}) due to a decrease in c_{p01h} as we change the mainstream gas properties from those for combustion products to those for air. There are second order contributions of positive sign from increases in $h_c(x)$ and $\lambda(x)$ and of negative sign from a decrease in $\bar{k}_w(x)$ as we change from combustion products to air.

The surface-mean changes in overall cooling effectiveness as we move from combustion products to air, $\overline{\Delta\theta}_{GP}$, were +0.016, +0.013, +0.013, +0.014 and +0.013 for TRs 2.0, 1.8, 1.6, 1.4 and 1.2, respectively. As percentages of the mean effectiveness for the cases with combustion products at each TR (0.463, 0.462, 0.457, 0.450 and 0.441 for TRs 2.0, 1.8, 1.6, 1.4 and 1.2, respectively), these equate to changes of +3.45%,+2.86%, +2.85%, +3.02% and +3.06%.

So far as the trends with surface distance are concerned, the change in overall cooling effectiveness, $\Delta\theta_{GP}(x)$ is approximately constant with surface distance. This is explained by a balance between two primary effects. The first effect—in isolation—would drive a reduction in the magnitude of $\Delta\theta_{GP}(x)$ with surface distance because the *absolute* increase in $\eta_{ML}(x)$ as we change from combustion products to air is greater at the LE than the TE (see full discussion of this effect in the context of Figs. 8 and 11). The second effect—in isolation—would drive an increase in the magnitude of $\Delta\theta(x)$ with surface distance because the *absolute* decrease in $h_m(x)$ as we change from combustion products to air is greater at the TE than LE. This second effect occurs primarily because the absolute decrease in both $k_m(x)$ and $c_{pm}(x)$ is greater at the TE than LE due to an increase in the ratio $\dot{m}_e(x)/\dot{m}_{1c}$ i.e. an increase in entrainment rate with surface distance (recall that $k_m(x)$ and $c_{pm}(x)$ are evaluated as mass average values at the local mixing layer temperature T_m).

In summary, the effect of changing from combustion products to air is an increase in $\theta(x)$. This is caused by the combined effects of a decrease in $h_m(x)$ and an increase in $\eta_{ML}(x)$. There are second order contributions of positive sign from increases in $h_c(x)$ and $\lambda(x)$ and negative sign from a decrease in $\bar{k}_w(x)$.

Results IX: Engine-to-Rig Scaling Example

We now consider the overall correction offset for scaling from typical engine conditions to typical laboratory conditions. We look at an example where we move from typical engine condition of $T_{01h} = 1750$ K and $T_{02c} = 875$ K (i.e. TR = 2.0) and combustion products to typical lab conditions of $T_{01h} = 360$ K and $T_{02c} = 300$ K (i.e. TR = 1.2). We do this two ways. In the first method (M1) we sum correction offsets for: TR effects in air between the reference TR and TR = 1.2 (i.e. the result of Fig. 8 in Results II); effect of moving from high *absolute* temperature to low absolute temperature, $\Delta\theta_{ABS}^{TR=2.0}(x)$ (i.e. the result of Fig. 28 in Results IV) for TR = 2.0; and the effect of moving from gas properties for combustion products to gas properties for air for TR = 2.0, $\Delta\theta_{GP}^{TR\,=\,2.0}(x)$ (i.e. the result of Fig. 29 in Results VII). We refer to the sum of these effects for this engine-to-rig scaling as $\Delta\theta_{E-R}^{M1}(x)$ where $\Delta\theta_{E-R}^{M1}(x) = \Delta\theta(x) + \Delta\theta_{ABS}^{TR=2.0}(x) + \Delta\theta_{GP}^{TR=2.0}(x)$. The individual terms and the sum are shown in Fig. 30. The sign convention is inherited from the underlying terms, and is such that $\Delta\theta_{E-R}^{M1}(x)$ should be added to the engine condition to scale to the rig condition. In the second method (M2) we directly compute the engine condition and the rig condition and take the difference. We refer to this as $\Delta\theta_{E-R}^{M2}(x)$. The sign convention is as for $\Delta\theta_{E-R}^{M1}(x)$. This ends up being mathematically identical to the first method because the two simulations of method 2 form a subset of the four simulations of method 1 i.e. it is merely a consistency check. This is also shown in Fig. 30. In this example we use the system 1 network with the fixed-PR domain-global BC.

Looking at Fig. 30 we first note that methods M1 and M2 give identical results, showing consistency ($\Delta\theta_{E-R}^{M1}(x) = \Delta\theta_{E-R}^{M2}(x) = \Delta\theta_{E-R}(x)$). The overall engine-to-rig correction is negative in sign, increasing from LE to TE in an approximately linear manner over most of the range of surface distance, and with average value $\overline{\Delta\theta}_{E-R} = -0.0042$ (−0.84% of $\bar{\theta} = 0.5$). For the purpose of scaling between engine and rig results it is a welcome co-incidence that the relatively large (in absolute terms) correction offsets sum to a small value.

To provide a look-up graph that may be of practical use, we repeat this analysis for all TR in the range $1.1 \le TR \le 2.0$, to

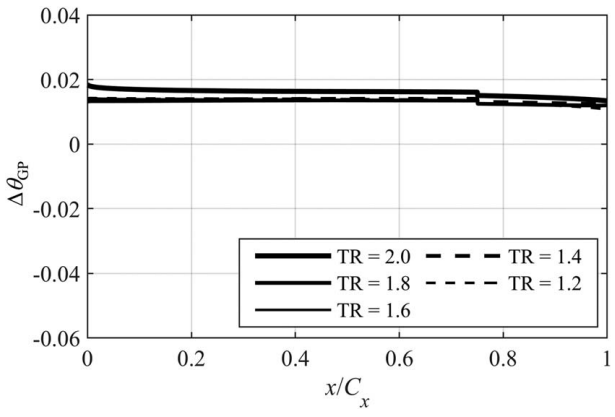

Fig. 29 Distributions of change in overall cooling effectiveness, $\Delta\theta_{GP}(x)$, as we change from fluid properties for combustion products to those for air at fixed TR (in range $1.2 \le TR \le 2.0$) as a function of normalised surface distance, x/C_x (system 1 and domain-global boundary conditions of fixed PR)

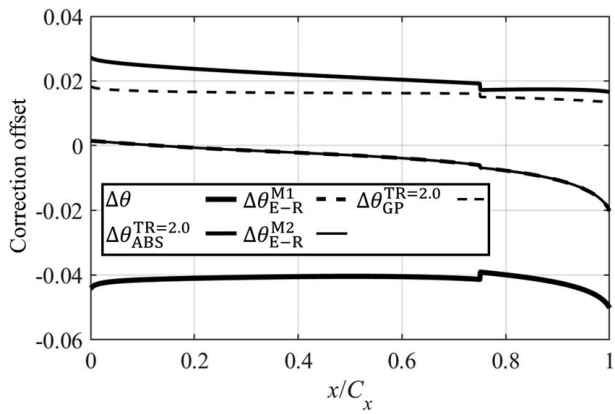

Fig. 30 Example of engine-to-rig scaling offsets calculated using two methods: a superposition approach $\Delta\theta_{E-R}^{M1}(x) = \Delta\theta(x) + \Delta\theta_{ABS}^{TR=2.0}(x) + \Delta\theta_{GP}^{TR=2.0}(x)$; and a direct simulation approach $\Delta\theta_{E-R}^{M2}(x)$

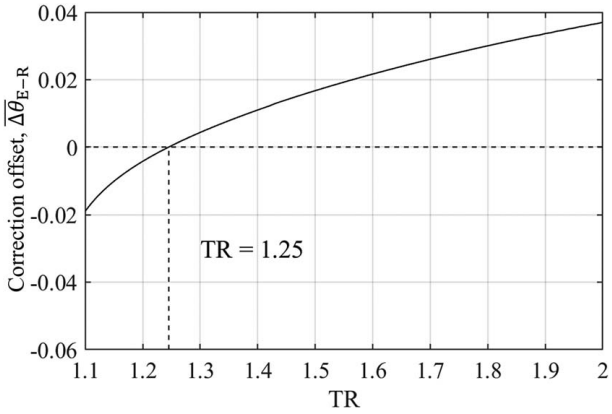

Fig. 31 Overall engine-to-rig correction offset $\overline{\Delta\theta}_{E-R}$ as a function of TR

calculate the characteristic $\overline{\Delta\theta}_{E-R} = f(\mathrm{TR})$. For each TR, the trend with surface distance is the sum of the line for the relevant TR from Fig. 8, the line TR = 2.0 from Fig. 28, and the line TR = 2.0 from Fig. 29. The surface-mean value is given as a function of TR in Fig. 31. The correction offset is approximately −0.019 for TR = 1.1, and approximately +0.037 for TR = 2.0, and has a decreasing gradient with TR as TR increases. For TR = 1.25 the characteristic has a value of zero.

The conclusion is that laboratory experiments can both underestimate or over-estimate engine values of overall cooling effectiveness but only by a very small margin. Testing at TR = 1.25 there is no required correction offset between rig and engine conditions. For practical purposes this can be regarded as a key result of this paper.

Results X: Sensitivity to Definitions of Overall Cooling Effectiveness

In this section we consider the sensitivity of our results to the definition of overall cooling effectiveness. Our results—so far—have been presented in terms of the following definition of overall cooling effectiveness (Eq. (2))

$$\theta(x) = \frac{c_h(x)T_{01h} - T_{w1}(x)}{c_h(x)T_{01h} - c_c(x)T_{02c}}$$

This is our preferred definition because it has three particular advantages. Firstly, it limits the range of θ to $0.0 \le \theta \le 1.0$. This is so because of the following theoretically limiting temperatures: a theoretical maximum external temperature of $c_h(x)T_{01h}$ in the case of no cooling flow and an adiabatic wall; a theoretical minimum external temperature of $c_c(x)T_{02c}$ for the case of perfect cooling (no entrained hot gas) and an adiabatic wall. Secondly, the definition of Eq. (2) accounts for compressibility effects in the hot stream and mixing layer through the use of the recovery ratios $c_h(x)$ and $c_c(x)$. The third advantage of this definition is the close parallel with our definition of η_{ML}, which was defined so as to limit the range of η_{ML} to $0.0 \le \eta_{ML} \le 1.0$ and to account for compressibility effects in the hot stream and mixing layer. We note that Michaud et al. [24] used the same definition (Eq. (2)) but their recovery ratio distribution, $c_c(x)$, was calculated using the Mach number distribution associated with a mixing layer with entrainment rate distribution that satisfied a particular desired distribution of $\eta_{ML}(x)$. In our case, the recovery ratio distribution was calculated using the Mach number distribution associated with a *hypothetical perfect cooling film* (no entrainment). This very subtle distinction ensures that θ is *strictly* limited to the range $0.0 \le \theta \le 1.0$. This pedantic distinction arises because of the co-dependence of Mach number distribution and entrainment rate because the external static pressure distribution is affected by the mass flow rate (and corresponding cross-sectional area) of the mixing layer.

Taking the change in overall cooling effectiveness with TR (result of Fig. 9) we compute the surface-mean, $\overline{\Delta\theta}$, for each TR, and plot this as a function of TR (i.e. $\overline{\Delta\theta} = f(\mathrm{TR})$) in Fig. 32. The trend is non-linear, with an increase in gradient as we move from the reference TR to lower-than-reference TR. We now compare this trend with trends arising from three other definitions of overall film cooling effectiveness.

In previous work from the same group (see Kirollos et al. [6] and Michaud et al. [25]) an alternative definition of effectiveness has been used, in which the terms $c_h(x)T_{01h}$ and $c_c(x)T_{02c}$ in the denominator are replaced by T_{01h} and T_{02c}, giving

$$\theta'(x) = \frac{c_h(x)T_{01h} - T_{w1}(x)}{T_{01h} - T_{02c}} \tag{37}$$

i.e. total temperatures are used in place of recovery temperatures in the denominator. Justifications for using T_{02c} instead of $c_c(x)T_{02c}$ in the denominator might be as follows: firstly, within the cooling duct the flow is entirely incompressible, so any effect in the conjugate system arising from the *internal cooling* is associated with a limiting temperature unaffected by compressibility (recovery) effects; on the external wall the only region in which compressibility effects are significant (the late surface) is one in which η_{ML} takes low values (very dilute cooling flow in the mixing layer). The fundamental justification for using T_{01h} in place of $c_h(x)T_{01h}$ in the denominator is less clear, but likely arises from historical convention. The trend for the average change (from the reference TR) in $\theta'(x)$ with TR ($\overline{\Delta\theta'}$) is shown, as a function of TR, in Fig. 32. The trend is extremely similar to that for $\overline{\Delta\theta}$. This can be understood by performing a similar analysis to that leading to Eq. (11), but for $\theta'(x)$, through which we can show that we render $\theta'(x)$ into the form $\theta'(x) = \beta_1(x)\theta(x)$ where $\beta_1(x) = (c_h(x)\mathrm{TR} - c_c(x))/(\mathrm{TR} - 1)$. We see that over a wide range of TR $\beta_1 \cong 1$, giving $\theta' \cong \theta$.

Although there is little difference in practice between using θ' and θ, we feel that θ' is incomplete for two reasons: it does not make use of the two theoretically limiting temperatures and therefore does not constrain overall cooling effectiveness between 0 and 1; it has a weaker parallel with our definition of η_{ML} (see Eq. (3)).

A third definition which is probably that in widest use (see, for example, Albert and Bogard [9], Williams et al. [26], Nathan et al. [27] and Dyson et al. [28]) is one in which recovery temperatures are used in neither the numerator or denominator. It is

$$\theta''(x) = \frac{T_{01h} - T_{w1}(x)}{T_{01h} - T_{02c}} \tag{38}$$

We dislike this parameter because it fails to account for compressibility and does not use either of the two limiting temperatures in the system. This means both that overall cooling effectiveness is

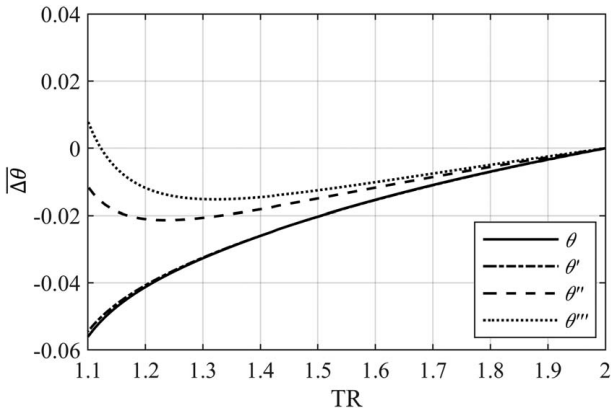

Fig. 32 Magnitude of surface-mean of the change in overall cooling effectiveness, $\overline{\Delta\theta}$, as a function of TR, for four definitions of overall cooling effectiveness

not constrained to a rational range, and that artificial sensitivity to TR is introduced (we discuss this in a moment). The trend for the average change (from the reference TR) in $\theta''(x)$ with TR ($\overline{\Delta\theta''}$) is shown, as a function of TR, in Fig. 32. As we move from the reference TR to lower-than-reference TR, $\overline{\Delta\theta''}$ decreases from zero (by definition) at TR = 2.0, to a minimum at TR = 1.24. Below TR = 1.24, $\overline{\Delta\theta''}$ increases asymptotically to a limiting TR of unity. This can be understood by performing a similar analysis to that leading to Eq. (11), but for θ', through which we render $\theta''(x)$ into the form $\theta''(x) = \beta_1(x)\theta(x) + \beta_2(x)$ where $\beta_2(x) = (1 - c_h(x))$ TR/(TR − 1). We see that, as we decrease TR towards unity, $\beta_2(x)$ increases asymptotically. The combination of a reduction in $\theta(x)$ and increase in $\beta_2(x)$ as we decrease TR leads to the trend for $\overline{\Delta\theta''}$ in Fig. 32. Using this common definition the correction $\overline{\Delta\theta''}$ *explodes* at low TR as an artefact of failing to include compressibility in the definition.

Finally, consider a definition proposed by Luque et al. [5], which included a so-called recovery and redistribution parameter, $\mathfrak{R}(x)$, designed to account for compressibility effects and the redistribution of heat transferred from the compressible external flow domain to the supposedly (i.e. notwithstanding the transfer of heat from the compressible side, which—in fact—is coupling to a compressible region) incompressible internal flow domain. The definition of overall cooling effectiveness, $\theta'''(x)$, was

$$\theta'''(x) = \frac{\mathfrak{R}(x)T_{01h} - T_{w1}(x)}{\mathfrak{R}(x)T_{01h} - T_{02c}} \tag{39}$$

This defines an overall cooling effectiveness that is invariant of TR for the particular case *of all other non-dimensional groups being fixed as TR is varied.* This situation is of theoretical interest, but does not correspond to the typical engine-to-rig scaling problem, in which non-dimensional groups *vary sympathetically with TR* (key distinction with this study). We plot this for completeness in Fig. 32.

In summary, we see that our results are highly dependent on the definition of overall cooling effectiveness, and care needs to be given to the definition of this parameter. There are rational reasons to use a fully compressible form of this parameter and we recommend the form of Eq. (2).

Conclusions

In this paper we consider the relationship between overall cooling effectiveness (or so-called *metal effectiveness*) and mainstream-to-coolant total temperature ratio (TR). We consider the problem using both fundamental scaling arguments and using results from a low-order numerical model. Results have been presented for three different cooling system networks, and two types of domain-global BCs (the macro-boundary-conditions relevant to laboratory or engine tests).

The key conclusion of the paper is that (for low absolute temperature and for air) overall cooling effectiveness decreases as we move from the reference TR to lower-than-reference TR. Moving between a typical engine temperature ratio of 2.0 to a typical laboratory temperature ratio of 1.2 leads to a change in effectiveness of approximately −0.040 for a mean effectiveness of 0.500. This is equivalent to a −8% change. The rate of change accelerates with decreasing temperature ratio. The result was surprisingly insensitive to the cooling system network and the type of domain-global boundary conditions imposed. When the changes due to both *absolute* temperature and combustion products are considered (the engine-to-rig scaling problem) the correction offset can be both positive or negative, with a sweet-spot at TR = 1.25, for which the correction offset is zero.

We argue using a simple zero-dimensional model that the overall cooling effectiveness can be expressed—crudely—as a function of five local surface boundary conditions, and that insights can be gained by decomposing results into contributions arising from each. There is some dependence of the results on the type of domain global boundary conditions. For the fixed-PR BC, a reduction in θ is caused by reductions in η_{ML}, λ and an increase in h_m as we move from the reference TR to lower-than-reference TR whilst the contributions from changes in $\bar{k}_w$ and h_c are second order. For the BC of fixed exit Re *and* fixed PR, a reduction in θ is caused by a combination of reductions in η_{ML}, λ, h_m and h_c as we move from the reference TR to lower-than-reference TR, whilst the contribution from changes in $\bar{k}_w$ was small.

There are six supplementary conclusions:

(1) *Sensitivity to domain-global BCs.* The change in θ as we move from the reference TR to lower-than-reference TR was relatively insensitive to the domain-global BCs. This means the general results are applicable to both fixed PR and fixed exit Re *with* fixed PR BCs.

(2) *Sensitivity to mean value of overall cooling effectiveness.* The change in θ as we move from the reference TR to lower-than-reference TR was relatively insensitive to the value of $\bar{\theta}$ at the reference TR. This means the general results are applicable to a wide range of $\bar{\theta}$ values.

(3) *Sensitivity of results to internal cooling system network.* The change in θ as we move from the reference TR to lower-than-reference TR was highly insensitive to the details of the internal cooling network (mean corrections $\Delta\theta^{TR=1.2}$ were within 0.64% of each other for three cooling network styles). This means that the general results are applicable to a wide range of internal cooling networks.

(4) *Sensitivity to absolute temperature.* The effect *at fixed TR* of moving from high absolute temperature (engine conditions) to low absolute temperature (rig conditions) is an increase in the mean value of θ. For engine conditions of temperature ratio and absolute temperature ($T_{01h} = 1750$ K, $T_{02c} = 875$ K), there is a mean change in θ of +0.021 (+4.2% of $\bar{\theta} = 0.5$) when moving to rig conditions of absolute temperature ($T_{01h} = 600$ K, $T_{02c} = 300$ K). The implication is that overall cooling effectiveness is overestimated at lower absolute temperatures by typically 4.38%.

(5) *Combustion product effects.* The effect *at fixed TR* of changing gas properties for the mainstream gas from combustion products (engine conditions) to air (rig conditions) at high absolute temperature is an increase in θ. At engine conditions of temperature ratio, there is a mean change in θ of +0.016 (+3.2% of $\bar{\theta} = 0.5$). Overall cooling effectiveness is overestimated by using air instead of combustion products.

(6) *Engine-to-rig scaling.* Taking the effect of TR, absolute temperature, and combustion products together, laboratory experiments can under-estimate or over-estimate overall cooling effectiveness. Moving from engine conditions of temperature ratio, absolute temperature and mainstream gas properties, to rig conditions in the range $1.2 < TR < 1.4$, there is a mean change in θ which falls in the range $-0.005 < \overline{\Delta\theta} < 0.011$, i.e. within 2.2% of $\bar{\theta} = 0.5$. That is, the correction is small for the typical laboratory range. There is a sweet-spot for TR = 1.25, at which condition the correction offset between engine and rig conditions is zero. For practical purposes this can be regarded as a key result of this paper.

(7) *Sensitivity to definitions of overall cooling effectiveness.* The variation of overall cooling effectiveness with TR is highly dependent on the definition of overall cooling effectiveness used, and care needs to be given to the definition of this parameter. There are compelling rational reasons to use a fully compressible form of this parameter and we recommend the form of Eq. (2)

We believe this is the first paper to systematically quantify and explain from first principles the effect of TR on overall cooling effectiveness. We do so for a number of cooling system networks and for domain-global boundary conditions relevant to laboratory and engine testing. The resulting scaling charts allow scaling of

overall effectiveness data between typical low-temperature-ratio laboratory tests and engine temperature ratios.

Acknowledgment

The financial support of EPSRC is gratefully acknowledged.

Conflict of Interest

There are no conflicts of interest.

Data Availability Statement

The authors attest that all data for this study are included in the paper.

Nomenclature

Romans

A = cross-sectional area, m^2
Bi = Biot number, –
C_x = plate surface length, m
c = recovery ratio, –
c_c = recovery ratio of a hypothetical unmixed coolant stream with adiabatic wall condition, –
c_p = specific heat capacity, constant pressure, J kg^{-1} K^{-1}
c_{p0} = specific heat capacity at constant pressure evaluated at T_0, J kg^{-1} K^{-1}
c_v = specific heat capacity, constant volume, J kg^{-1} K^{-1}
d = film cooling hole diameter, m
D = hydraulic diameter, m
f_c = friction factor of the internal cooling channel, –
H = internal cooling channel height, m
h_c = internal heat transfer coefficient, W m^{-2} K^{-1}
h_m = external heat transfer coefficient, W m^{-2} K^{-1}
k = thermal conductivity, W m^{-1} K^{-1}
$\bar{k}_w$ = local through-wall average wall thermal conductivity, W m^{-1} K^{-1}
k_1 = multiplication factor used in modified mixing layer effectiveness correlation, –
k_2 = multiplication factor used in modified external Nusselt number correlation, –
k_3 = multiplication factor used in modified internal Nusselt number correlation, –
K = multiplication factor used in Nusselt number correlation for system 2, –
M = Mach number, –
$\dot{m}$ = mass flow rate, kg s^{-1}
$\dot{m}_e$ = integrated entrainment mass flow rate distribution, kg s^{-1}
$\dot{m}_h$ = mainstream mass flow rate, kg s^{-1}
$\dot{m}_m$ = integrated mixing layer mass flow rate, kg s^{-1}
Nu = Nusselt number, –
Nu'_c = modified cooling-channel Nusselt number, –
Nu'_m = modified external Nusselt number, –
Pr = Prandtl number, –
p = static pressure, Pa
p_0 = total pressure, Pa
$\dot{q}_m$ = external-side heat flux, W m^{-2}
R = specific gas constant, J kg^{-1} K^{-1}
$\mathfrak{R}$ = recovery and redistribution parameter, –
Re = Reynolds number, –
r = recovery factor, –
t_w = wall thickness, m
T = static temperature, K
T_0 = total temperature, K
T_{aw} = adiabatic wall temperature, K
T_w = wall temperature, K
$T_{\mathfrak{R}}$ = recovery and redistribution temperature, K
u = velocity, m s^{-1}
u'_{1c} = coolant velocity at film cooling hole exit, m s^{-1}
w = plate width, m
x = surface co-ordinate, m
x' = local surface co-ordinate based on stream-wise distance from the channel inlet, m
y = surface-normal co-ordinate, m

Greek Symbols

β_1 = multiplication factor in equation for θ', –
β_2 = multiplication factor in equation for θ'', –
γ = ratio of specific heat capacities, –
Δ = change in quantity, –
$\Delta\theta$ = change in overall cooling effectiveness as TR is varied, –
$\Delta\theta_{ABS}$ = change in overall cooling effectiveness as temperature is varied from high absolute temperature to low absolute temperature at fixed TR, –
$\Delta\theta_{E-R}$ = overall engine-to-rig correction, –
$\Delta\theta^{M1}_{E-R}$ = overall engine-to-rig correction (method 1), –
$\Delta\theta^{M2}_{E-R}$ = overall engine-to-rig correction (method 2), –
$\Delta\theta_{GP}$ = change in overall cooling effectiveness as fluid properties of mainstream are varied from combustion products to air at fixed TR, –
ε = total non-dimensional external-side heat flux between any location and the cooling channel inlet, –
η_{aw} = adiabatic film effectiveness, –
η_{ML} = effectiveness of the mixing layer, –
η'_{ML} = modified effectiveness of the mixing layer, –
θ = overall cooling effectiveness, –
θ_{Air} = overall cooling effectiveness for air, –
θ_{CP} = overall cooling effectiveness for combustion products, –
θ_{LT} = overall cooling effectiveness at low absolute temperature, –
θ_{HT} = overall cooling effectiveness at high absolute temperature, –
λ = internal cooling effectiveness, –
μ = dynamic viscosity, Pa s
ρ = density, kg m^{-3}
ρ'_{1c} = coolant density at film cooling hole exit, kg m^{-3}
φ = internal surface effectiveness, –

Subscripts

1 to 3 = plane numbers
1c = leading-circuit exit conditions
1h = mainstream inlet conditions
2c = cooling system inlet conditions
3c = coolant exit conditions
3h = mainstream exit conditions
3m = mixing layer exit conditions
c = internal coolant conditions
e = entrained hot-gas conditions
E1 to E5 = effects
h = mainstream conditions
j = effect index
m = mixing layer conditions
w = wall conditions
w1 = wall external surface conditions
w2 = wall internal surface conditions

Abbreviations

CMPR = coolant-to-mainstream pressure ratio, –
HPNGV = high-pressure nozzle guide vane
PR = overall total-to-static pressure ratio, –
TE = trailing edge
TR = mainstream-to-coolant temperature ratio, –

References

[1] Ornano, F., and Povey, T., 2020, "Theory of Non-Dimensional Groups in Film Effectiveness Studies," ASME J. Turbomach., **142**(4), p. 041002.

[2] Eckert, E. R. G., 1992, "Similarity Analysis of Model Experiments for Film Cooling in Gas Turbines," Wärme- und Stoffübertragung, **27**(4), pp. 217–223.

[3] Baldauf, S., and Scheurlen, M., 1996, "CFD Based Sensitivity Study of Flow Parameters for Engine Like Film Cooling Conditions," Proceedings of the ASME 1996 International Gas Turbine and Aeroengine Congress and Exhibition, Birmingham, UK, June 10–13, ASME Paper No. 96-GT-310.

[4] Greiner, N. J., Polanka, M. D., and Rutledge, J. L., 2015, "Scaling of Film Cooling Performance From Ambient to Engine Temperatures," ASME J. Turbomach., **137**(7), p. 071007.

[5] Luque, S., Jones, T. V., and Povey, T., 2016, "Theory for the Scaling of Metal Temperatures in Cooled Compressible Flows," Int. J. Heat Mass Transfer, **102**(8), pp. 331–340.

[6] Kirollos, B., Lubbock, R., Beard, P., Goenaga, F., Rawlinson, A., Janke, E., and Povey, T., 2017, "ECAT: An Engine Componenet Aerothermal Facility at the University of Oxford," Proceedings of the ASME Turbo Expo 2017: Turbomachinery Technical Conference and Exposition, Charlotte, NC, June 26–30, ASME Paper No. GT2017-64736.

[7] Luque, S., Jones, T. V., and Povey, T., 2017, "Scaling of Turbine Metal Temperatures in Cooled Compressible Flows—Experimental Demonstration of a New Theory," ASME J. Turbomach., **139**(8), p. 081001.

[8] Sweeney, P. C., and Rhodes, J. F., 2000, "An Infrared Technique for Evaluating Turbine Airfoil Cooling Designs," ASME J. Turbomach., **122**(1), pp. 170–177.

[9] Albert, J. E., and Bogard, D. G., 2013, "Measurements of Adiabatic Film and Overall Cooling Effectiveness on a Turbine Vane Pressure Side With a Trench," ASME J. Turbomach., **135**(5), p. 051007.

[10] Rutledge, J. L., Polanka, M. D., and Greiner, N. J., 2017, "Computational Fluid Dynamics Evaluations of Film Cooling Flow Scaling Between Engine and Experimental Conditions," ASME J. Turbomach., **139**(2), p. 021004.

[11] Fischer, J. P., McNamara, L. J., Rutledge, J. L., and Polanka, M. D., 2020, "Scaling Flat-Plate, Low-Temperature Adiabatic Effectiveness Results Using the Advective Capacity Ratio," ASME J. Turbomach., **142**(8), p. 081010.

[12] McNamara, L. J., Fischer, J. P., Rutledge, J. L., and Polanka, M. D., 2021, "Scaling Considerations for Thermal and Pressure-Sensitive Paint Methods Used to Determine Adiabatic Effectiveness," ASME J. Turbomach., **143**(1), p. 011004.

[13] Bryant, C. E., and Rutledge, J. L., 2023, "Theoretical Considerations for Scaling Convection in Overall Effectiveness Experiments," ASME J. Turbomach., **145**(1), p. 011007.

[14] Kirollos, B., and Povey, T., 2014, "Reverse-Pass Cooling Systems for Improved Performance," ASME J. Turbomach., **136**(11), p. 111004.

[15] McAdams, W. H., 1942, *Heat Transmission*, 2nd ed., McGraw-Hill Book Company, Inc., New York and London.

[16] Bergman, T. L., Lavine, A. S., Incropera, F. P., and Dewitt, D. P., 2011, *Fundamentals of Heat and Mass Transfer*, 7th ed., John Wiley & Sons, Inc., Hoboken, NJ.

[17] Kirollos, B., and Povey, T., 2015, "An Energy-Based Method for Predicting the Additive Effect of Multiple Film Cooling Rows," ASME J. Turbomach., **137**(12), p. 122607.

[18] Vinton, K. R., Watson, T. B., Wright, L. M., Crites, D. C., Morris, M. C., and Ardeshir, R., 2017, "Combined Effects of Freestream Pressure Gradient and Density Ratio on the Film Cooling Effectiveness of Round and Shaped Holes on a Flat Plate," ASME J. Turbomach., **139**(4), p. 041003.

[19] Cumpsty, N. A., and Heyes, A. L., 2015, *A Simple Guide to the Aerodynamics and Thermodynamic Design and Performance of Jet Engines*, 3rd ed., Cambridge University Press, USA.

[20] Zielińska, M., Yavorska, M., Poręba, M., and Sieniawski, J., 2010, "Thermal Properties of Cast Nickel Based Superalloys," Arch. Mater. Sci. Eng., **44**(1), pp. 35–38.

[21] Rhee, D., Kang, Y. S., Cha, B. J., and Lee, S., 2017, "Overall Cooling Effectiveness Measurements on Pressure Side Surface of the Nozzle Guide Vane With Optimized Film Cooling Hole Arrangements," Proceedings of the ASME 2017: Turbomachinery Technical Conference and Exposition, Charlotte, NC, June 26–30, ASME Paper No. GT2017-63421.

[22] Poferl, D. J., Svehla, R. A., and Lewandowski, K., 1969, "Thermodynamic and Transport Properties of Air and the Combustion Products of Natural Gas and of ASTM-A-1 Fuel With Air," National Aeronautics and Space Administration, Washington, D. C., NASA Report No. NASA TN D-5452.

[23] Oldfield, M. L. G., and Guo, S. M., 1997, "Aero-thermal Properties of Foreign Gas (SF6/AR) and Air: Recommended Formulae From 160 1000 K," OUEL Report No. 2141/97. Department of Engineering Science, University of Oxford, Oxford, UK.

[24] Michaud, M., Chowdhury, N. H. K., and Povey, T., 2023, "Experimental Study of Impact of In-Service Deterioration on Thermal Performance of High-Pressure Nozzle Guide Vanes," ASME J. Turbomach., **145**(2), p. 021014.

[25] Michaud, M., Ornano, F., Chowdhury, N. H. K., and Povey, T., 2020, "Methodology for High-Accuracy Infrared Calibration Environments With Through-Wall Heat Flux," J. Glob. Power Propuls. Soc., **4**, pp. 1–13.

[26] Williams, R. P., Dyson, T. E., Bogard, D. G., and Bradshaw, S. D., 2014, "Sensitivity of the Overall Cooling Effectiveness to Film Cooling and Internal Cooling on a Turbine Vane Suction Side," ASME J. Turbomach., **136**(3), p. 031006.

[27] Nathan, M. L., Dyson, T. E., Bogard, D. G., and Bradshaw, S. D., 2014, "Adiabatic and Overall Effectiveness for the Showerhead Film Cooling of a Turbine Vane," ASME J. Turbomach., **136**(3), p. 031005.

[28] Dyson, T. E., Bogard, D. G., Piggush, J. D., and Kohli, A., 2013, "Overall Effectiveness for a Film Cooled Turbine Blade Leading Edge With Varying Hole Pitch," ASME J. Turbomach., **135**(3), p. 031011.